Chemical Research in Toxicology

pubs.acs.org/crt

Article

A Promising Resveratrol Analogue Suppresses CSCs in Non-Small-Cell Lung Cancer via Inhibition of the ErbB2 Signaling Pathway

Tanapon Soonthonsrima,[⊥] Ismail Dwi Putra,[⊥] Preeyaphan Phookphan,[⊥] Zin Zin Ei,[⊥] Masashi Yokoya, and Pithi Chanvorachote*,[⊥]

Cite This: *Chem. Res. Toxicol.* 2025, 38, 415−432

Read Online

ACCESS | Metrics & More | Article Recommendations | Supporting Information

ABSTRACT: The ErbB2 signaling pathway plays a crucial role in cancer stem cells (CSCs), governing cancer aggressiveness and proliferation. Targeting ErbB2 holds promise for advancing cancer therapeutics. Resveratrol (RES) and its derivatives have been noted for their ability to target proteins that are involved in CSCs. In this investigation, we synthesize novel derivatives of RES, aim at elucidating structure−activity relationships (SARs) that could enhance the anticancer properties of the RES analogues, and explore their capacities to suppress CSCs. YI-12, an O-benzyl-substituted 1,3-diphenylpropane, demonstrated the most potent anticancer activity against lung cancer cells (A549 and H460), showing high potential inhibiting cancer colony formation. Interestingly, not only does YI-12 suppress CSCs-related proteins, indicated by decreased expression of CSC-enhancing molecules such as CD133-, OCT4-, and CSC-related protein β-catenin, but it also induces apoptosis in CSC-rich spheroids after treatment. Additionally, molecular docking and bioinformatic analysis suggest ErbB2 as a potential target of the compound with a strong binding affinity (−6.709 kcal/mol) compared to the reference compound TAK-285 (−5.563 kcal/mol). YI-12's capability to bind and inhibit ErbB2 leads to the suppression of PI3K and AKT. In conclusion, we highlight the novel resveratrol derivative YI-12 for its ability to inhibit CSCs through the ErbB2 signaling pathway. This compound represents a promising structure that should be further developed for potential use in anticancer therapy.

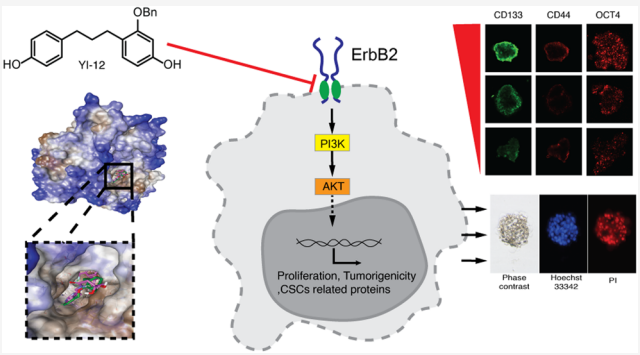

INTRODUCTION

Over the past decades and in the foreseeable future, cancer remains a noninfectious disease widespread globally. Alarmingly, it caused over 10 million people deaths in 2022 and is projected to rise to 30 million by 2050.[1,2] Lung cancer accounts for nearly 20% of all cancer cases.[2] Additionally, the discovery of new drugs significantly lags behind the rate at which cancer cells develop drug resistance.[3] Studies indicate that the failure of cancer treatments is often due to the development of cancer stem cells (CSCs), which contribute to drug resistance in tumor progression.[4,5]

CSCs are a unique subset of cancer cells that possess stem cell-like properties, including self-renewal and the ability to initiate tumors.[6] Recent research highlights CSCs as promising targets for cancer therapy, as targeting the molecular signaling pathways associated with CSCs could inhibit their activity and improve treatment outcomes.[6−9] Targeting CSCs has shown promise in recurrence. CSCs are often identified by markers like CD133, which is linked to chemotherapy resistance and poor prognosis in lung cancer.[10,11] Other important markers include transcription factors such as OCT4, NANOG, SOX2, and the glycoprotein CD44, which play crucial roles in CSC functions.[12]

Recently, there has been an effort to identify drugs that can target CSCs by modulating various proteins such as AKT,[13] PI3K,[14] and β-catenin,[15] which are key components of different signaling pathways. However, several studies have shown that drug resistance can develop against these targeted proteins, necessitating the use of multiple drugs in combination for effective treatment.[16] Nevertheless, developing a single drug with the efficacy to inhibit CSCs would be a more effective strategy than relying on combination therapies. One promising approach involves targeting receptors on the cell surface such as EGFR, C-met, and ErbB2 (HER2). However, not all oncogenic diverted proteins, including human epidermal growth factor receptor 2 (ErbB2/HER2) currently, have approved targeted therapies. The ErbB family, also known as epidermal growth factor (EGF) receptors, belongs to subclass 1 of the receptor tyrosine kinase (RTK) superfamily.

Received: October 15, 2024
Revised: February 18, 2025
Accepted: February 20, 2025
Published: February 25, 2025

This family comprises four distinct members: ErbB1 (also known as EGFR or HER1), ErbB2 (HER2/neu), ErbB3 (HER3), and ErbB4 (HER4).[17,18] ErbB2 typically forms heterodimers with other members of the HER receptor family or homodimers when overexpressed. This dimerization leads to the phosphorylation of tyrosine residues and activation of downstream tumorigenic signaling pathways, such as PI3K-AKT pathways.[17−19] Additionally, it has been reported that the stabilization of ErbB2 promotes a stem cell-like phenotype in lung adenocarcinoma cells,[20] making them more resistant to treatment. Historically, therapies targeting ErbB2 have been used predominantly in the treatment of breast cancer. Recently, these therapies have also been applied to lung cancer treatment. Consequently, current market offerings and drug development still involve the combined use of ErbB2-targeted drugs with EGFR-targeted therapies.[17,21] Unfortunately, previous research has demonstrated that ErbB2-targeted monoclonal antibodies and traditional pan-HER tyrosine kinase inhibitors (TKIs) have exhibited limited antitumor effectiveness in treating non-small-cell lung cancer (NSCLC) with HER2 alterations.[19,22] Consequently, it is essential to identify and develop new therapeutic agents to improve treatment outcomes.

Currently, CSC inhibitors are largely derived from natural sources, such as medicinal plants or marine organisms, and there is a strong interest in using natural products for therapeutic purposes. One such compound is resveratrol trans-3,5,4′-trihydroxystilbene (RES), a natural polyphenol known for its powerful antioxidant effects, which holds promise for suppressing CSCs.[13,23] However, RES faces challenges such as limited solubility in water and poor bioavailability.[24] An earlier study has demonstrated that structural modifications of RES can substantially improve its water solubility and bioavailability.[13] Due to these challenges, the study of modifying the structure of RES has garnered significant interest. Research has shown that replacing hydroxyl groups with methoxy groups can enhance the compound's anticancer properties.[13,25] Additionally, adjusting the hydroxyl groups on the phenol ring of stilbenes and methylating these hydroxyl groups not only increases the compound's bioavailability but also improves its solubility.[26,27] In a previous study conducted by our research group, we examined the effects of various RES analogues on lung cancer cell inhibition. The study revealed that these analogues could increase binding affinity.[13] Additionally, the RES analogues were developed thus far have shown specificity for proteins such as AKT and mTOR.[13,28] However, there have been no reports of RES analogues targeting the ErbB2/HER2 signaling pathway.

In this study, we aim to demonstrate that RES analogue can effectively inhibit the initiation and growth of CSCs by targeting ErbB2, a protein that regulates the PI3K signaling pathway. The effectiveness of the RES analogue YI-12 in inhibiting growth and suppressing CSC phenotypes was evaluated and compared across different lung cancer cell lines. Furthermore, we provided evidence that YI-12 interacts with ErbB2 through a molecular docking study. We strongly anticipate that this research will pave the way for future anticancer therapy and the clinical development of this compound.

EXPERIMENTAL SECTION

Reagents and Antibodies. Roswell Park Memorial Institute (RPMI) 1640 medium, Dulbecco's modified Eagle's medium (DMEM), L-glutamine, and Antibiotic-Antimycotic (100X) (Anti-Anti) were procured from Gibco (Grand Island, NY). Fetal bovine serum (FBS), phosphate-buffered saline (PBS), and 0.25% trypsin-EDTA were acquired from HyClone (Logan, UT). RES, 3-(4,5-dimethylthiazol-2-yl)-2,5-diphenyltetrazolium bromide (MTT), dimethyl sulfoxide (DMSO), crystal violet, paraformaldehyde, Hoechst 33342, and propidium iodide (PI) were sourced from Sigma-Aldrich (St. Louis, MO). Radioimmunoprecipitation assay (RIPA) lysis buffer and Immobilon Western Chemiluminescent HRP Substrate were obtained from Millipore (Billerica, MA), while the protease inhibitor cocktail was procured from Roche Molecular Biochemicals (Indianapolis, IN).

The primary antibody utilized in this investigation is detailed in Table S1, and the secondary antibodies, antirabbit IgG (#7074) or antimouse IgG (#7076), were supplied by Cell Signaling Technology (Danvers, MA).

Synthesis of Resveratrol Analogue YI. *2-Hydroxy-4-(methoxymethoxy)benzaldehyde (**2**).*[29] A solution of **1** (690.6 mg, 5.0 mmol) in CH_2Cl_2 (16 mL) was added *i*-Pr_2NEt (940 mL, 5.5 mmol, 1.1 equiv) and MOMCl (415 mL, 5.5 mmol, 1.1 equiv) at 0 °C. The reaction mixture was stirred for 1 h at room temperature, and the reaction mixture was diluted with H_2O (10 mL), extracted with CH_2Cl_2 (20 mL × 3), washed with brine, dried over anhydrous Na_2SO_4, and concentrated. The crude product was purified over a SiO_2 column (*n*-hexane/EtOAc = 7:3) to give **2** (714.0 mg, 78%) as a yellow solid.

^1H NMR (400 MHz, $CDCl_3$) δ: 11.37 (1H, s), 9.74 (1H, s), 7.45 (1H, d, J = 8.5 Hz), 6.65 (1H, dd, J = 2.2, 8.5 Hz), 6.60 (1H, d, J = 2.2 Hz), 5.22 (2H, s), 3.49 (3H, s).

*2-(Benzyloxy)-4-(methoxymethoxy)benzaldehyde (**3**).*[30] A solution of **2** (1.38 g, 7.57 mmol) in acetone (150 mL) was added K_2CO_3 (2.60 g, 18.93 mmol, 2.5 equiv) and benzyl bromide (990 mL, 8.33 mmol, 1.1 equiv), and the obtained solution was refluxed for 2 h. After cooling to room temperature, the reaction mixture was filtered, and the obtained filtrate was evaporated under vacuum. The residue was purified over a SiO_2 column ($CHCl_3$) to give **3** (2.06 g, 100%) as a yellow oil.

^1H NMR (400 MHz, $CDCl_3$) δ: 10.40 (1H, s), 7.82 (1H, d, J = 9.3 Hz), 7.33−7.46 (5H, m), 6.68−6.70 (2H, m), 5.21 (2H, s), 5.16 (2H, s), 3.48 (3H, s).

*Diethyl-(4-hydroxybenzyl)phosphonate (**5**).*[31] A solution of **4** (1.00 g, 8.06 mmol) in Et_2O (45 mL) was added to PBr_3 (990 μL, 10.42 mmol, 1.29 equiv) at 0 °C. The reaction mixture was stirred for 1 h at the same temperature. The reaction mixture was diluted with H_2O (50 mL), extracted with EtOAc (100 mL × 3), washed with brine, dried over anhydrous Na_2SO_4, and concentrated to give bromide solution in EtOAc. Then, $P(OEt)_3$ (1750 μL, 10.11 mmol, 1.25 equiv) and crude bromide solution were mixed and concentrated to remove EtOAc. The reaction mixture was stirred for 3.5 h at 140 °C. The reaction mixture was concentrated in vacuo, and the residue was purified over a SiO_2 column (*n*-Hexane/EtOAc = 1:3) to give **5** (1.34 g, 68%) as a pale orange solid.

^1H NMR (400 MHz, $CDCl_3$) δ: 7.57 (1H, s), 7.05 (2H, dd, J = 2.7, 8.5 Hz), 6.64 (2H, d, J = 7.8 Hz), 4.00−4.09 (4H, m), 3.06 (2H, d, J = 21.0 Hz), 1.26 (6H, t, J = 7.0 Hz).

*Diethyl-{4-(methoxymethoxy)benzyl}phosphonate (**6**).*[31] A solution of **5** (855.6 mg, 3.5 mmol) in CH_2Cl_2 (14 mL) was added *i*-Pr_2NEt (1.65 mL, 9.7 mmol, 2.8 equiv) and MOMCl (730 mL, 9.7 mmol, 2.8 equiv) at 0 °C. The reaction mixture was stirred for 22 h at room temperature, and the reaction mixture was diluted with H_2O (35 mL), extracted with CH_2Cl_2 (70 mL × 3), washed with brine, dried over anhydrous Na_2SO_4, and concentrated. The crude product was purified over SiO_2 column ($CHCl_3$/EtOAc = 1:1) to give **6** (722.9 mg, 72%) as a colorless oil.

^1H NMR (400 MHz, $CDCl_3$) δ: 7.23 (2H, dd, J = 2.7, 8.8 Hz), 6.98 (2H, d, J = 8.9 Hz), 5.16 (2H, s), 3.95−4.08 (4H, m), 3.47 (3H, s), 3.09 (2H, d, J = 21.2 Hz), 1.25 (6H, t, J = 7.1 Hz).

*(E)-2-(Benzyloxy)-4-(methoxymethoxy)-1-{4-(methoxymethoxy)-styryl}benzene (**7, YI-1**).* A solution of **6** (127.0 mg, 0.44 mmol, 1.2 equiv) in THF (2.0 mL) was stirred at −78 °C and added *t*-BuOK

https://doi.org/10.1021/acs.chemrestox.4c00436
Chem. Res. Toxicol. 2025, 38, 415−432

solution in THF (590 μL, 0.59 mmol, 1.6 equiv., 1.0 M) over 30 min. The reaction mixture was stirred for 20 min at the same temperature and added **3** (100.5 mg, 0.37 mmol) in THF (2.0 mL) over 20 min, and the mixture was stirred for 1 h at −78 °C and for 10 min at 0 °C. Then, the reaction mixture was stirred for 17 h at room temperature. The reaction mixture was cooled to 0 °C and diluted with saturated NH_4Cl solution, extracted with EtOAc (60 mL × 3), washed with saturated NH_4Cl solution and H_2O, dried over anhydrous Na_2SO_4, and concentrated. The crude product was purified over a SiO_2 column (CH_2Cl_2) to give YI-1 (**7**) (99.8 mg, 67%) as a pale yellow oil.

^{1}H NMR (400 MHz, $CDCl_3$) δ: 7.24−7.50 (9H, m), 7.01 (1H, d, *J* = 16.3 Hz), 7.00 (2H, d, *J* = 8.7 Hz), 6.65−6.68 (2H, m), 5.17 (2H, s), 5.16 (2H, s), 5.11 (2H, s), 3.48 (3H, s), 3.47 (3H, s). ^{13}C NMR (100 MHz, $CDCl_3$) δ: 157.7 (C), 156.9 (C), 156.5 (C), 136.9 (C), 132.2 (C), 128.6 (CH), 127.9 (CH), 127.5 (CH), 127.4 (CH), 127.2 (CH), 127.0 (CH), 121.7 (CH), 121.1 (CH), 116.4 (CH), 108.3 (CH), 101.8 (CH), 94.5 (CH_2), 94.4 (CH_2), 70.5 (CH_2), 56.04 (CH_3), 55.98 (CH_3). IR (KBr): 3020, 1607, 1510, 1217, 1153, 1079, 1014, 772, 669, 494 cm^{-1}. HRMS (ESI): calcd for $C_{25}H_{26}O_5Na$, 429.1678; found: $[M + Na]^+$ 429.1673.

*5-(Methoxymethoxy)-2-(4-(methoxymethoxy)phenethyl)phenol (**8**).* A solution of **7** (366.0 mg, 0.90 mmol) in THF (45 mL) was hydrogenated over 10% Pd/C (55% water, 191.7 mg) at room temperature for 3 h. The catalyst was removed by Celite filtration, and the filtrate was concentrated in vacuo. The crude product was purified over SiO_2 column (*n*-Hexane/EtOAc = 2:1) to give **8** (238.9 mg, 83.0%) as a yellow solid.

^{1}H NMR (400 MHz, $CDCl_3$) δ: 7.11 (2H, d, *J* = 8.6 Hz), 6.98 (1H, d, *J* = 8.0 Hz), 6.96 (2H, d, *J* = 8.6 Hz), 6.55 (1H, dd, *J* = 2.4, 8.2 Hz), 6.49 (1H, d, *J* = 2.4 Hz), 5.16 (2H, s), 5.12 (2H, s), 5.02 (1H, s), 3.48 (3H, s), 3.47 (3H, s), 2.77−2.85 (4H, s). ^{13}C NMR (100 MHz, $CDCl_3$) δ: 156.5 (C), 155.4 (C), 154.3 (C), 135.5 (C), 130.7 (CH), 129.4 (CH), 121.5 (C), 116.3 (CH), 108.4 (CH), 103.9 (CH), 94.6 (CH_2), 94.5 (CH_2), 55.94 (CH_3), 55.91 (CH_3), 35.5 (CH_2), 31.8 (CH_2). IR (KBr): 3348, 2946, 1617, 1509, 1442, 1231, 1146, 1071, 1028, 901, 837, 560, 506 cm^{-1}. HRMS (ESI): calcd for $C_{18}H_{22}O_5Na$, 341.1365; found: $[M + Na]^+$ 341.1364.

*2-(Benzyloxy)-4-(methoxymethoxy)-1-(4-(methoxymethoxy)-phenethyl)benzene (**9**, **YI-3**).* A solution of **8** (10.0 mg, 0.03 mmol) in acetone (2.0 mL) was added K_2CO_3 (11.0 mg, 0.08 mmol, 2.6 equiv) and benzyl bromide (4.1 mL, 0.035 mmol, 1.1 equiv), and the obtained solution was refluxed for 23.5 h. After cooling to room temperature, the reaction mixture was filtered, and the obtained filtrate was evaporated under vacuum. The crude product was purified over SiO_2 column (*n*-Hexane/EtOAc = 3:1) to give **9** (11.3 mg, 88%) as a colorless oil.

^{1}H NMR (400 MHz, $CDCl_3$) δ: 7.31−7.46 (5H, m), 7.06 (2H, d, *J* = 8.6 Hz), 7.02 (1H, d, *J* = 8.2 Hz), 6.92 (2H, d, *J* = 8.6 Hz), 6.66 (1H, d, *J* = 2.4 Hz), 6.58 (1H, dd, *J* = 2.3, 8.1 Hz), 5.14 (4H, s), 5.05 (2H, s), 3.48 (3H, s), 3.47 (3H, s), 2.78−2.88 (4H, m). ^{13}C NMR (100 MHz, $CDCl_3$) δ: 157.3 (C), 156.7 (C), 155.3 (C), 137.2 (C), 136.0 (C), 130.2 (CH), 129.4 (CH), 128.5 (CH), 127.8 (CH), 127.3 (CH), 124.2 (C), 116.1 (CH), 107.4 (CH), 101.3 (CH), 94.7 (CH_2), 94.6 (CH_2), 69.9 (CH_2), 56.0 (CH_3), 55.9 (CH_3), 35.8 (CH_2), 32.5 (CH_2). IR (KBr): 2930, 1610, 1588, 1509, 1454, 1381, 1232, 1151, 1078, 1016, 922, 828, 739, 697 cm^{-1}. HRMS (ESI): calcd for $C_{25}H_{28}O_5Na$, 431.1834; found: $[M + Na]^+$ 431.1830.

*1-{4-(Methoxymethoxy)phenyl}ethan-1-one (**11**).*[32] A solution of **10** (408.5 mg, 3.00 mmol) in CH_2Cl_2 (10 mL) was added *i*-Pr_2NEt (765 mL, 4.50 mmol, 1.5 equiv) and MOMCl (338.6 mL, 4.50 mmol, 1.5 equiv) at 0 °C. The reaction mixture was stirred for 1 h at room temperature, and the reaction mixture was diluted with H_2O (20 mL), extracted with CH_2Cl_2 (20 mL × 3), washed with brine, dried over anhydrous Na_2SO_4, and concentrated. The crude product was purified over SiO_2 column (*n*-hexane/EtOAc = 7:3) to give **11** (449.1 mg, 83%) as a colorless oil.

^{1}H NMR (400 MHz, $CDCl_3$) δ: 7.93 (2H, d, *J* = 8.8 Hz), 7.07 (2H, d, *J* = 8.8 Hz), 5.39 (2H, s), 3.48 (3H, s), 2.56 (3H, s).

*(E)-3-{2-(Benzyloxy)-4-(methoxymethoxy)phenyl}-1-{4-(methoxymethoxy)phenyl}prop-2-en-1-one (**12**).* A solution of **3** (131.3 mg, 0.48 mmol) and **11** (86.5 mg, 0.48 mmol, 1.0 equiv) in MeOH (3.5 mL) was added to NaOH (38.3 mg, 0.97 mmol, 2.0 equiv), and the obtained solution was stirred for 96 h at the room temperature. The reaction mixture was diluted with H_2O (20 mL), extracted with CH_2Cl_2 (30 mL × 3), washed with brine, dried over anhydrous Na_2SO_4, and concentrated. The crude product was purified over SiO_2 column (*n*-hexane/EtOAc = 7:3) to give **12** (121.1 mg, 58%) as a yellow solid.

^{1}H NMR (400 MHz, $CDCl_3$) δ: 7.96 (1H, d, *J* = 15.8 Hz), 7.80 (2H, d, *J* = 8.9 Hz), 7.68 (1H, d, *J* = 15.5 Hz), 7.51−7.52 (3H, m), 7.41−7.46 (3H, m), 7.00 (2H, d, *J* = 8.9 Hz), 6.73 (1H, d, *J* = 2.0 Hz), 6.70 (1H, dd, *J* = 2.3, 8.3 Hz), 5.24 (2H, s), 5.24 (2H, s), 5.14 (2H, s), 3.50 (3H, s), 3.49 (3H, s). ^{13}C NMR (100 MHz, $CDCl_3$) δ: 189.4 (C), 160.6 (C), 160.1 (C), 160.0 (C), 140.2 (CH), 136.2 (C), 132.7 (CH), 132.5 (C), 130.6 (CH), 128.8 (CH), 128.3 (CH), 128.1 (CH), 121.3 (CH), 118.3 (C), 115.6 (CH), 108.2 (CH), 101.2 (CH), 94.3 (CH_2), 94.1 (CH_2), 70.6 (CH_2), 56.25 (CH_3), 56.23 (CH_3). IR (KBr): 3072, 2901, 2823, 1655, 1604, 1314, 1247, 1173, 1079, 1030 cm^{-1}. EI-MS *m*/*z* (%): 434 (M^+, 3), 272 (43), 180 (25), 91 (100), 45 (53). HRMS (EI): calcd for $C_{26}H_{26}O_6$, 434.1729; found: *m*/*z* 434.1731.

*(E)-3-(2-(Benzyloxy)-4-hydroxyphenyl)-1-(4-hydroxyphenyl)-prop-2-en-1-one (**26**, **YI-10**).* A solution of **12** (43.6 mg, 0.10 mmol) in EtOH (4.0 mL) was added to HCl (4.0 μL), and the obtained solution was refluxed for 2 h. The reaction mixture was diluted with *sat.* $NaHCO_3$ (10 mL), extracted with EtOAc (20 mL × 3), washed with H_2O (10 mL), dried over anhydrous Na_2SO_4, and concentrated. The crude product was purified over SiO_2 column ($CHCl_3$/EtOAc = 9:1) to give **YI-10** (**13**) (28.1 mg, 81%) as an orange solid.

^{1}H NMR (400 MHz, CD_3OD) δ: 7.91 (1H, d, *J* = 15.6 Hz), 7.69 (1H, d, *J* = 15.6 Hz), 7.70 (2H, d, *J* = 9.0 Hz), 7.53−7.56 (2H, m), 7.49 (1H, d, *J* = 8.4 Hz), 7.39−7.47 (3H, m), 6.78 (2H, d, *J* = 8.8 Hz), 6.59 (1H, d, *J* = 2.2 Hz), 6.48 (1H, dd, *J* = 2.2, 8.4 Hz), 5.13 (2H, s). ^{13}C NMR (100 MHz, CD_3OD) δ: 191.6 (C), 163.5 (C), 162.9 (C), 161.7 (C), 142.1 (CH), 138.1 (C), 134.1 (CH), 132.0 (CH), 131.3 (C), 129.8 (CH), 129.40 (CH), 129.35 (CH), 120.3 (CH), 117.0 (C), 116.3 (CH), 109.5 (CH), 101.2 (CH), 71,7 (CH_2). IR (KBr): 3317, 1638, 1604, 1551, 1459, 1262, 1212, 1167, 1018, 979, 834, 732 cm^{-1}. HRMS (ESI): calcd for $C_{22}H_{17}O_4$, 345.1127; found: $[M-H]^-$ 345.1130.

*5-(Methoxymethoxy)-2-[3-{4-(methoxymethoxy)phenyl}propyl]-phenol (**14**).* A solution of **12** (30.9 mg, 0.07 mmol) in THF (4.0 mL) was hydrogenated over 10% Pd/C (55% water, 15.4 mg) at room temperature for 26 h. The catalyst was removed by Celite filtration and the filtrate was concentrated in vacuo. The crude product was purified over SiO_2 column ($CHCl_3$/EtOAc = 19:1) to give **14** (19.0 mg, 83.0%) as a yellow oil.

^{1}H NMR (400 MHz, $CDCl_3$) δ: 7.11 (2H, d, *J* = 8.6 Hz), 6.99 (1H, d, *J* = 8.3 Hz), 6.96 (2H, d, *J* = 8.3 Hz), 6.55 (1H, dd, *J* = 2.3, 8.3 Hz), 6.50 (1H, d, *J* = 2.0 Hz), 5.15 (2H, s), 5.12 (2H, s), 4.94 (1H, s), 3.48 (3H, s), 3.47 (3H, s), 2.61 (2H, t, *J* = 7.7 Hz), 2.56 (2H, t, *J* = 7.7 Hz), 1.86−1.92 (2H, m). ^{13}C NMR (100 MHz, $CDCl_3$) δ: 156.4 (C), 155.3 (C), 154.2 (C), 135.8 (C), 130.6 (CH), 129.3 (CH), 121.7 (C), 116.2 (CH), 108.4 (CH), 103.8 (CH), 94.6 (CH_2), 94.6 (CH_2), 56.0 (CH_3), 55.9 (CH_3), 34.7 (CH_2), 31.5 (CH_2), 28.8 (CH_2). IR (KBr): 3397, 2932, 1615, 1510, 1443, 1279, 1231, 1152, 1077, 1014, 922, 839, 756, 652 cm^{-1}. EI-MS *m*/*z* (%): 332 (M^+, 100), 256 (86), 167 (22), 123 (27), 45 (63). HRMS (EI): calcd for $C_{19}H_{24}O_5$, 332.1624; found: *m*/*z* 332.1622.

*2-(Benzyloxy)-4-(methoxymethoxy)-1-[3-{4-(methoxymethoxy)-phenyl}propyl]benzene (**15**).* A solution of **14** (196.2 mg, 0.59 mmol) in acetone (20 mL) was added K_2CO_3 (205.5 mg, 1.49 mmol, 2.5 equiv) and benzyl bromide (77 mL, 0.65 mmol, 1.1 equiv), and the obtained solution was refluxed for 24 h. After cooling to room temperature, the reaction mixture was filtered, and the obtained filtrate was evaporated under vacuum. The residue was purified over a SiO_2 column (*n*-hexane/EtOAc = 7:3) to give **15** (225.3 mg, 90%) as a colorless oil.

^{1}H NMR (400 MHz, $CDCl_3$) δ: 7.31−7.42 (5H, m), 7.07 (2H, d, *J* = 8.3 Hz), 7.03 (1H, d, *J* = 8.3 Hz), 6.92 (2H, d, *J* = 8.0 Hz), 6.64

https://doi.org/10.1021/acs.chemrestox.4c00436
Chem. Res. Toxicol. 2025, 38, 415−432

(1H, d, J = 1.7 Hz), 6.59 (1H, dd, J = 1.4, 8.3 Hz), 5.139 (2H, s), 5.136 (2H, s), 5.04 (2H, s), 3.473 (3H, s), 3.472 (3H, s), 2.64 (2H, t, J = 7.7 Hz), 2.59 (2H, t, J = 7.7 Hz), 1.86−1.92 (2H, m, 2′-H). ^{13}C NMR (100 MHz, $CDCl_3$) δ: 157.3 (C), 156.6 (C), 155.2 (C), 137.3 (C), 136.1 (C), 130.2 (CH), 129.3 (CH), 128.5 (CH), 127.7 (CH), 127.2 (CH), 124.7 (C), 116.1 (CH), 107.4 (CH), 101.4 (CH), 94.7 (CH_2), 94.6 (CH_2), 69.8 (CH_2), 56.0 (CH_3), 55.9 (CH_3), 34.9 (CH_2), 31.7 (CH_2), 29.5 (CH_2). IR (KBr): 3017, 2932, 2853, 1217, 1152, 1118, 1078, 1016 cm^{-1}. EI-MS m/z (%): 423 (M^+, 24), 346 (16), 167 (27), 91 (100), 45 (37). HRMS (EI): calcd for $C_{26}H_{30}O_5$, 422.2093; found: m/z 422.2095.

*3-(Benzyloxy)-4-{3-(4-hydroxyphenyl)propyl}phenol (**16, YI-12**).* A solution of **15** (42.7 mg, 0.10 mmol) in EtOH (4.0 mL) was added to *conc* HCl (4.0 μL), and the obtained solution was refluxed for 1 h. The reaction mixture was diluted with *sat.* $NaHCO_3$ (10 mL), extracted with EtOAc (20 mL × 3), washed with H_2O (10 mL), dried over anhydrous Na_2SO_4, and concentrated. The crude product was purified over SiO_2 column (*n*-Hexane/EtOAc = 7:3) to give YI-12 (**16**) (35.5 mg, quant.) as a pale orange solid.

^{1}H NMR (400 MHz, CD_3OD) δ: 7.26−7.39 (5H, m), 6.93 (2H, d, J = 8.2 Hz), 6.89 (1H, d, J = 8.2 Hz), 6.66 (2H, d, J = 8.4 Hz), 6.44 (1H, d, J = 2.2 Hz), 6.31 (1H, dd, J = 2.3, 8.1 Hz), 4.98 (2H, s), 2.47−2.56 (4H, m), 1.76−1.83 (2H, m). ^{13}C NMR (100 MHz, CD_3OD) δ: 158.7 (C), 157.6 (C), 156.1 (C), 139.0 (C), 134.8 (C), 130.3 (CH), 129.5 (CH), 128.7 (CH), 128.2 (CH), 123.2 (C), 116.0 (CH), 108.0 (CH), 101.2 (CH), 70.8 (CH_2), 35.9 (CH_2), 33.6 (CH_2), 30.6 (CH_2). IR (KBr): 3252, 2922, 1609, 1512, 1447, 1231, 1173, 1112, 1038, 969, 833, 733 cm^{-1}. HRMS (ESI): calcd for $C_{22}H_{21}O_3$, 333.1491; found: $[M\text{-}H]^-$ 333.1495.

Cell Culture. Human lung cancer cell lines A549 and H460 were procured from the American Type Culture Collection (Manassas, VA). H460 cells were propagated in RPMI medium (Gibco), while A549 cells were cultured in DMEM (Gibco). The culture media were supplemented with 10% FBS (HyClone), 2 mM L-glutamine (Gibco), and 1x Anti-Anti (Gibco). Upon reaching 70−80% confluence, the cells were detached using 0.25% trypsin−EDTA (HyClone) and subcultured in the same media. Cell cultures were maintained at 37 °C in a humidified atmosphere with 5% CO_2.

Preparation of Compounds Solution. Stock solutions of RES and YI were prepared at a concentration of 50 mM in DMSO (Sigma) and stored in aliquots at −20 °C. Dilutions of RES and YI to achieve designated final concentrations ranging from 0 to 200 μM were made by using cell culture media for subsequent experiments. DMSO served as the vehicle control in these experiments.

Cell Viability Assay. The impact of RES and YI on cell viability in lung cancer cells was evaluated via an MTT assay. In brief, lung cancer cell lines (A549 and H460) were seeded overnight at a density of 1 × 10^4 cells/well in 96-well plates. Subsequently, the cells were treated with various concentrations (0−200 μM) of RES or YI for 24 h. Following the designated incubation period, an MTT solution (0.5 mg/mL) was added, and the cells were incubated in darkness for 3 h at 37 °C in a CO_2 incubator. The purple formazan crystals formed were dissolved by adding DMSO (100 μL/well). The absorbance was then measured at 570 nm using a microplate reader (PerkinElmer, Waltham, MA). The percentage of cell viability relative to the nontreated control was determined from the optical density (OD) ratio of treated to nontreated control cells. IC_{50} values were obtained through regression analysis of dose−response curves using GraphPad Prism9 software (San Diego). The cancer selectivity index (SI) was computed using the following equation: SI = mean IC_{50} against normal cells/mean IC_{50} against cancer cells.

Nuclear Staining Assay. Apoptosis and necrosis were detected by co-staining with Hoechst 33342 (Sigma Chemical, St. Louis, MO) and propidium iodide (PI) (Sigma Chemical, St. Louis, MO,). Nuclear morphology was assessed by using the DNA dye Hoechst 33342. The lung cancer cell lines (A549 and H460) were seeded in 96-well plates at 1.2 × 10^4 cells/well and treated with various concentrations (0−50 μM) of RES or YI for 24 h. Then, the treated cells were stained with 10 μM Hoechst 33342 and 5 μM PI at 37 °C for 10 min. The cells were visualized under a fluorescence microscope (Olympus DP70, Melville, NY) and the image analysis was performed and determined using ImageJ.[33]

Proliferation Assay. An MTT assay was employed to evaluate the antiproliferative impact of RES analogue, YI-12, over a period of three consecutive days. The NSCLC cell lines A549 and H460 were seeded at a cell density of 1 × 10^4 cells per well in a 96-well plate. The cells were exposed to low concentrations (0−50 μM) of YI-12 or RES at various time points (0, 24, 48, and 72 h) and then incubated under 5% CO_2 at 37 °C. Subsequently, the cell viability was assessed using an MTT assay at 0, 24, 48, and 72 h. The percentage of cell proliferation was determined by dividing the OD of the cells at each time point by the OD of the nontreated control cells.

Colony Formation Assay. NSCLC cell lines were seeded in triplicate into 6-well plates at a density of 300 cells per well. After overnight attachment, cells were exposed to varying concentrations (0−50 μM) of YI-12 or RES for 24 h. Following treatment, the medium containing YI-12 was replaced with a fresh medium. Colonies were allowed to form over a period of 7 days, with the medium refreshed every 2 days. For colony staining, colonies were washed once with PBS, fixed by adding fixative (methanol:acetic acid (3:1, v/v)) for 5 min, and then stained with crystal violet (0.05% (w/v)) in 4% paraformaldehyde for 30 min. Excess crystal violet was removed by washing with distilled water multiple times, and the colonies were allowed to air-dry at room temperature. Digital images of the colonies were captured using a digital camera, and the acquired images were analyzed using ImageJ software (National Institutes of Health (NIH), Bethesda, MD).

Western Blot Analysis. NSCLC cell lines were planted overnight. The cells were treated with YI-12 at 0−50 μM for 24 h. The following cells were lysed and prepared for Western blotting. Nonspecific binding was blocked with 5% skim milk before incubation with the primary antibody (CD133, OCT4, ALDH1A1, PI3K, p-PI3K, AKT, p-AKT, and GAPDH) at dilution 1:1000 overnight at 4 °C. The appropriate secondary antibody (goat antirabbit IgG (HRP) or rabbit antimouse IgG (HRP)) was diluted at dilution 1:5000 and incubated for 1 h at room temperature (RT). The enhanced chemiluminescence (Immobilon Western HRP Substrate, Millipore) was used to detect protein bands and analyzed by ImageJ (NIH, Bethesda, MD).

Immunofluorescence Assay. For staining of cell monolayers, A549 and H460 cells were seeded at a density of 1 × 10^4 cells per well in 96-well plates overnight. The cells were then treated with YI-12 or RES at 0−50 μM for 24 h. Following fixation with 4% paraformaldehyde for 15 min, cells were permeabilized with 0.2% (v/v) Triton X-100 and blocked with 10% (v/v) FBS for 20 min at RT. The cells were incubated overnight at 4 °C in the presence of CD44, CD133, OCT4, SOX2, ALDH1A1, PI3K, or p-PI3K primary antibodies at a dilution of 1:400 in 4% FBS. After incubation, Alexa Fluor 488 or Alexa Fluor 594 conjugated with goat antirabbit IgG secondary antibody at a ratio of 1:500 in 4% FBS was added and incubated for 1 h at RT in the dark. Cell nuclei were stained with Hoechst 33342 (10 μg/mL) for 15 min at RT and then photographed under confocal microscopy (Zeiss, Jena, Germany). The fluorescence intensity was measured using ImageJ software.

For staining spheroid (3D), A549 and H460 cells were allowed to form primary and secondary spheroids, as described before. At day 14 of secondary spheroid development, CSC-rich populations were treated with 0−50 μM YI-12 for 6 h, and then the cells were stained following the same procedure as described previously for cell monolayer staining.

Three-Dimensional (3D) CSC Spheroid Formation. Cells were seeded and treated with YI-12 or RES (0−50 μM) and then they were plated at a density of 5 × 10^3 cells per well in a 24-well ultralow attachment plate. Primary tumor spheroids were captured after incubation for 3 and 7 days with a phase-contrast microscope (Nikon ECLIPSE Ts2; Tokyo, Japan). Then, the spheroids were trypsinized and resuspended into a single cell. The 5 × 10^3 cells/mL were seeded onto 24-well ultralow attachment plates for 10 days to form secondary CSC-enriched spheroids and photographed on day 3, day 7, and day 10. The secondary spheroids were then transferred to a 96-well ultralow attachment plate, with one spheroid per well, and treated

https://doi.org/10.1021/acs.chemrestox.4c00436
Chem. Res. Toxicol. 2025, 38, 415−432

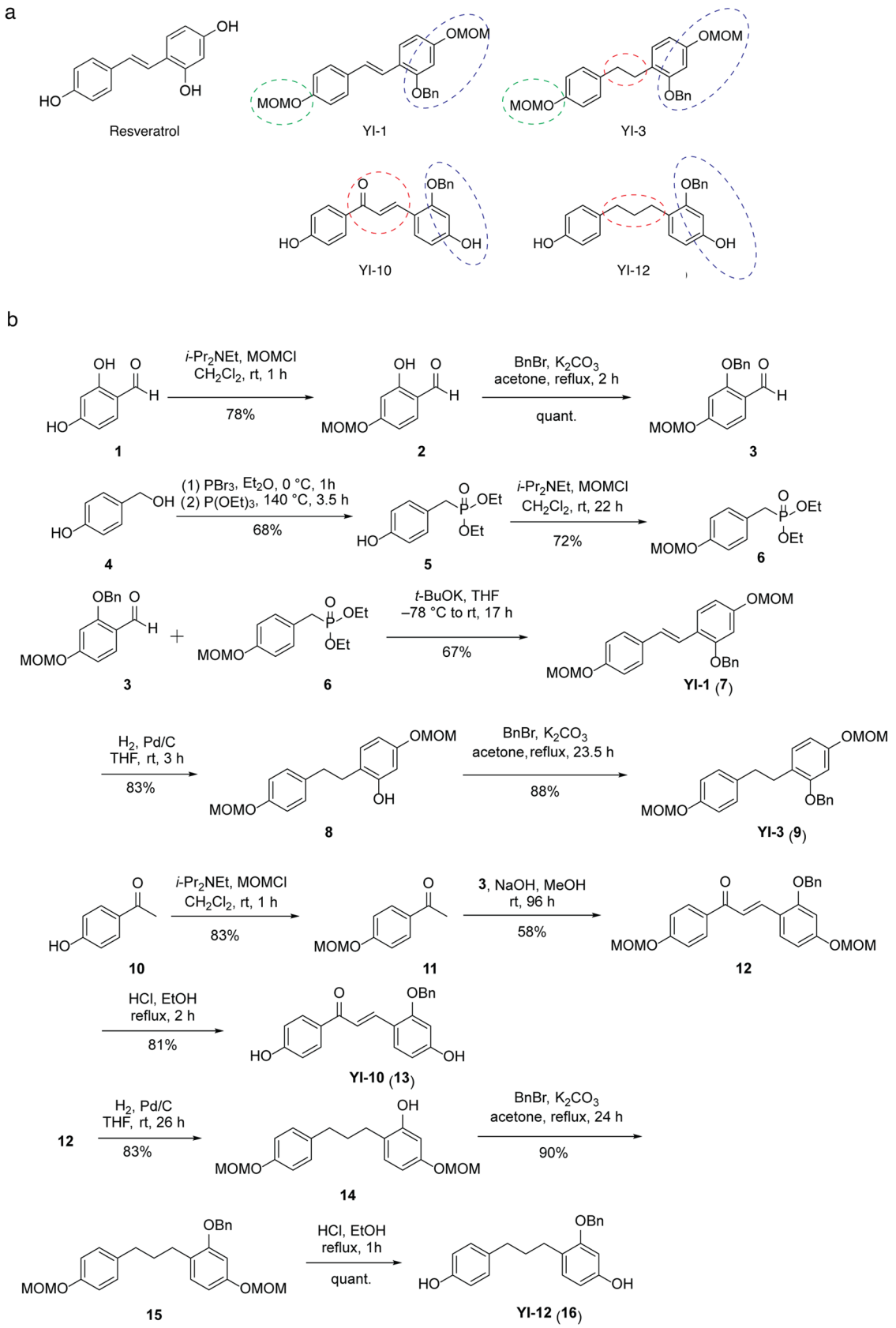

Figure 1. Derivatives of Resveratrol (RES): YI-1, YI-3, YI-10, and YI-12. (a) Core structure of RES. (b) Step-by-step synthesis for derivatives of RES (YI-1, YI-3, YI-10, and YI-12).

with various concentrations of YI-12. The survival of cells was monitored at 0, 0.5, and 2 h using an inverted microscope. The single spheroids were stained with Hoechst 33342 and PI for 15 min after 2 h, to assess their viability and proliferation, and imaged using a

https://doi.org/10.1021/acs.chemrestox.4c00436
Chem. Res. Toxicol. 2025, 38, 415−432

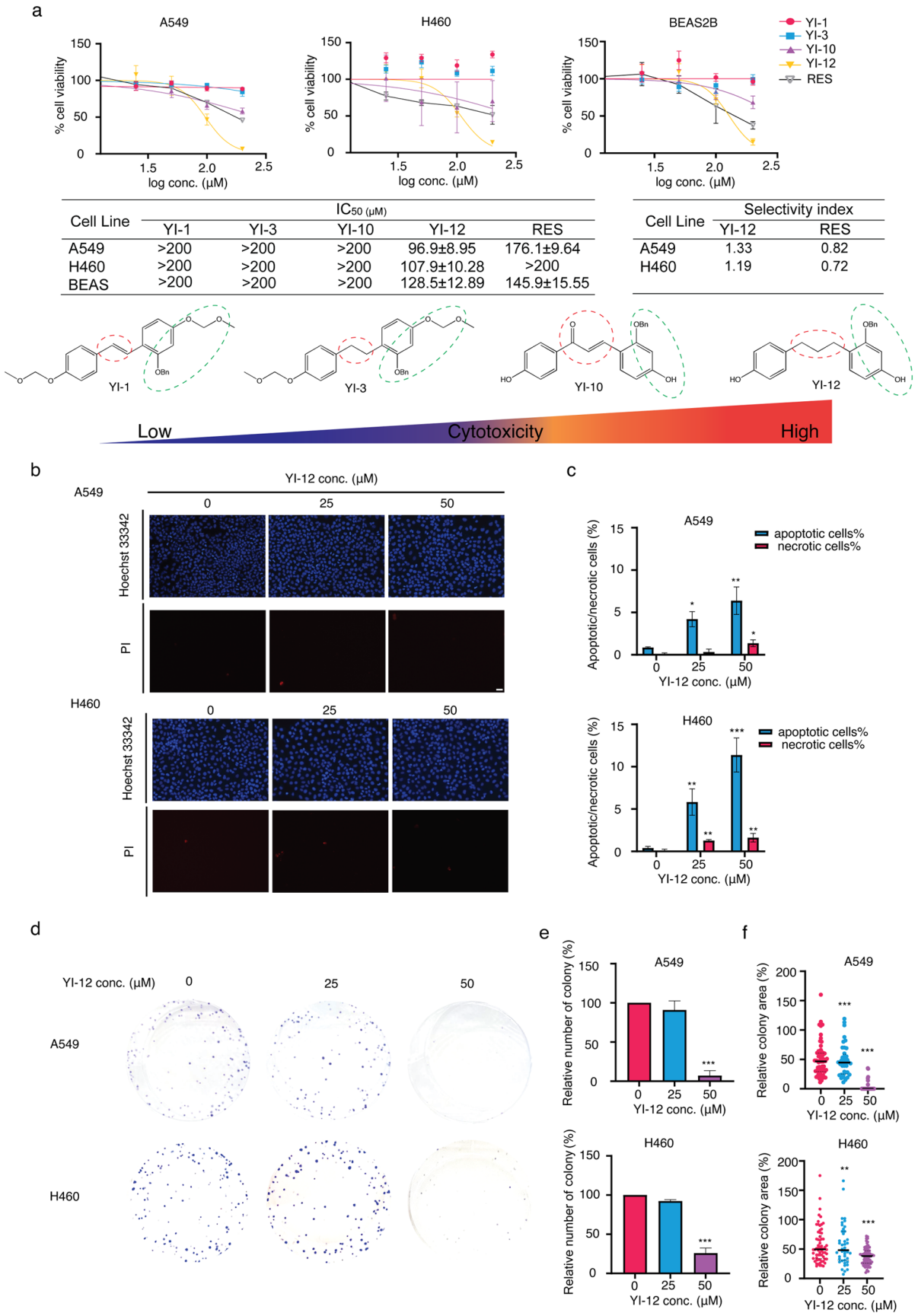

Cell Line	IC_{50} (μM)				
	YI-1	YI-3	YI-10	YI-12	RES
A549	>200	>200	>200	96.9±8.95	176.1±9.64
H460	>200	>200	>200	107.9±10.28	>200
BEAS	>200	>200	>200	128.5±12.89	145.9±15.55

Cell Line	Selectivity index	
	YI-12	RES
A549	1.33	0.82
H460	1.19	0.72

Figure 2. Screening of RES derivatives YI-1, YI-3, YI-10, and YI-12 for their effect on cell viability in lung cancer cells (A549, H460) and a nontumorigenic epithelial cell line derived from human bronchial epithelium (BEAS-2B) was conducted. (a) NSCLC cells were seeded and treated with RES and its derivatives (0−200 μM) for 24 h. An MTT assay was performed to determine the IC_{50} values for the RES derivatives in treating NSCLC cells. The selectivity index values were calculated relative to the parent RES compound, used as a positive control. (b, c) NSCLC cells were

https://doi.org/10.1021/acs.chemrestox.4c00436
Chem. Res. Toxicol. 2025, 38, 415−432

Figure 2. continued

seeded and treated with YI-12 (0−50 μM) for 24 h. Apoptotic and necrotic cells were evaluated by co-staining with Hoechst 33342 and PI, and images were captured using a fluorescence microscope. The percentages of apoptotic and necrotic cells were calculated. (d) Lung cancer cells were seeded and treated with YI-12 (0−50 μM) for 72 h. Colonies were allowed to grow for 7 days, stained with crystal violet, and counted to measure colony formation and area. (e) Percentages of colony numbers were calculated. (f) Relative colony area shown in the violin plot. Data are presented as the mean ± SD (n = 3). Significance is indicated by *, **, and *** representing statistically significant differences between treated and nontreated control cells at $p < 0.05$, $p < 0.01$, and $p < 0.001$, respectively.

fluorescence microscope (Olympus IX 51 with DP70; Olympus America, Inc., Center Valley, PA) or a confocal microscope (Zeiss, Jena, Germany).[34]

Network Pharmacology Analysis to Identify Potential Target of YI12. In this study, "Cancer stem cells" or "non-small-cell lung cancer" was used as a keyword to search to identify CSCs-related genes and NSCLCs-related genes in the GeneCards database (https://www.genecards.org/). Genes categorized as "Protein Coding" with a relevance score exceeding 5.0 were considered for further analysis. Finally, we built an NSCLCs/CSCs-related gene set by intersecting target genes of NSCLCs and CSCs.

To build a YI-12-related gene set, the pharmacological targets of Y−I12 were collected from Swiss Target Prediction (http://www.swisstargetprediction.ch/). A set of targets was obtained by intersecting the YI-12-related gene set and the NSCLCs/CSCs-related target genes (https://bioinfogp.cnb.csic.es/tools/venny/). The 67 targets were analyzed using the ShinyGO 0.80 for KEGG pathway.[35] The KEGG pathway analyses were considered to be significantly enriched with a false discovery rate (FDR) cutoff of 0.05. The STRING database (http://string-db.org/) was used to construct the protein−protein interaction (PPI) network. The parameter was specified as *Homo sapiens*, with a confidence level threshold set at 0.90 for higher reliability in STRING analysis. The PPI network was exported to the TSV format file and imported into the CytoHubba plugin within Cytoscape V3.9.1 (The Cytoscape Consortium, San Diego, CA) to identify the top 10 core targets. The DMNC algorithm was used as the primary parameter for ranking.[36]

Molecular Docking. Molecular docking of ligand(s) and proteins was conducted using AutoDock Vina1.2.5.[37,38] The ligand YI-12 was constructed and optimized by using Gaussian 16 at the B3LYP/6-31G(p) level of theory. Protein PDB files were obtained from the Protein Data Bank, with their respective PDB IDs listed in Table S2. Each protein was prepared by removing crystallized water molecules, ions, and other ligands, followed by proper protonation using PROPKA[39] to ensure accurate protonation states at physiological pH.

The center and size of the grid box for docking each protein were determined based on the known active site coordinates and are detailed in Table S2. Docking exhaustiveness was set to 32 (56 for PDB ID 3RCD), providing a thorough exploration of the binding site, and the number of ligand poses was set to 20 (50 for PDB ID 3RCD) to capture a diverse range of potential binding conformations. The pose with the lowest binding affinity, indicative of the highest binding strength, was selected for further analysis.

To visualize the results, two-dimensional (2D) and three-dimensional (3D) representations of the ligand-protein complexes were generated using Discovery Studio Visualizer 2020. Validation of the docking protocol was performed by redocking the cocrystallized ligand of each protein into their respective binding sites and comparing the predicted binding modes with experimental data, ensuring the reliability of the docking results.

Molecular Dynamic (MD) Simulation. Molecular dynamics (MD) simulations were performed using AMBER to evaluate the stability of the ligand-ErBb2 complex, as obtained from molecular docking. The protein was parametrized with the AMBER ff19SB force field, while the ligand was parametrized using the GAFF2 force field, based on RESP charges calculated from its geometry-optimized structure. The OPC water model was employed. The protein−ligand complex was solvated in a truncated octahedron box, neutralized with Na^+ or Cl^- ions, and NaCl was added to reach a concentration of 150 mM. The system was energy-minimized, heated to 310 K under NVT ensemble, and equilibrated under NPT conditions for 600 ps with a 2 fs time step. Production MD was conducted for 100 ns with a 2 fs time step, applying a 1.2 nm cutoff for nonbonded interactions and the Particle Mesh Ewald (PME) method for long-range electrostatics. Post simulation, trajectory analysis was performed to calculate backbone and ligand RMSD, RMSF, radius of gyration (R_g), and hydrogen bond count. The final 15 ns of the simulation was used to compute the solvated interaction energy.[40,41]

Statistical Analysis. All experiments were conducted with a minimum of three biological replicates, and the results are presented as the mean ± standard deviation. Statistical analyses were carried out using GraphPad Prism 9.0 (GraphPad Software, La Jolla, CA). The unpaired t test was used to compare statistical differences between two groups, while ANOVA was employed for comparisons among more than two groups. A significance level of $P < 0.05$ was considered statistically significant.

RESULTS

Synthesis of Resveratrol Derivative YI. In this present study, we investigated the anticancer activity of RES analogue YI against NSCLCs. The chemical structure of RES and its analogue is shown in Figure 1a. The RES analogues in this study were classified as stilbenes (**7**; YI-1), bibenzyl (**9**; YI-3), chalcones (**13**; YI-10), and diphenylpropane (**16**; YI-12). YI-3 and YI-12 were synthesized from the reduction of YI-1 and YI-10, respectively. YI-1 was synthesized from Horner−Wadsworth−Emmons reaction of β-resorcylaldehyde (2,4-dihydroxybenzaldehyde) derivative **3** and phosphonate of gastrodigenin (4-hydroxybenzyl alcohol) **6**, similar to our reported synthesis of moscatilin.[13] Meanwhile, YI-10 was synthesized through the Claisen-Schmidt condensation of **3** with MOM-protected 4-hydroxyacetophenone **11**. The MOM protecting group was kept in the structure for YI-1 and YI-3, while deprotection was performed for YI-10 and YI-12. The MOM protecting group was found to remain intact after catalytic hydrogenation using Pd/C, whereas the benzyl group was cleaved.

The synthesis successfully synthesized YI-1, YI-3, YI-10, and YI-12 with yields up to, respectively, 67, 88, 81, and 99.9%. The successful synthesis of YI-1 and YI-10 was characterized by the appearance of doublet peak in proton NMR with J-coupling value around 15−16 Hz, indicating the vicinal, trans proton. While the disappearance of those protons in YI-3 and YI-12 indicated the successful reduction of the vinyl group of YI-1 and YI-10. The full synthesis pathway of the compounds is shown in Scheme (Figure 1b)

Evaluation of Cytotoxicity through MTT Assay during Screening of Resveratrol Derivatives YI. The MTT assay was utilized to evaluate the cytotoxic ability of RES derivatives in A549 and H460 cancer cells at various concentrations over 24 h. The results indicated that compounds YI-1, YI-3, and YI-10 exhibited IC_{50} values of >200 μM for both A549 and H460 cells. In contrast, YI-12 demonstrated IC_{50} values of 96.9 ± 8.95 and 107.9 ± 10.28 μM for A549 and H460 cells, respectively. The results showed that YI-12 had the greatest efficacy among the RES analogues in lung cancer cell lines,

https://doi.org/10.1021/acs.chemrestox.4c00436
Chem. Res. Toxicol. 2025, 38, 415−432

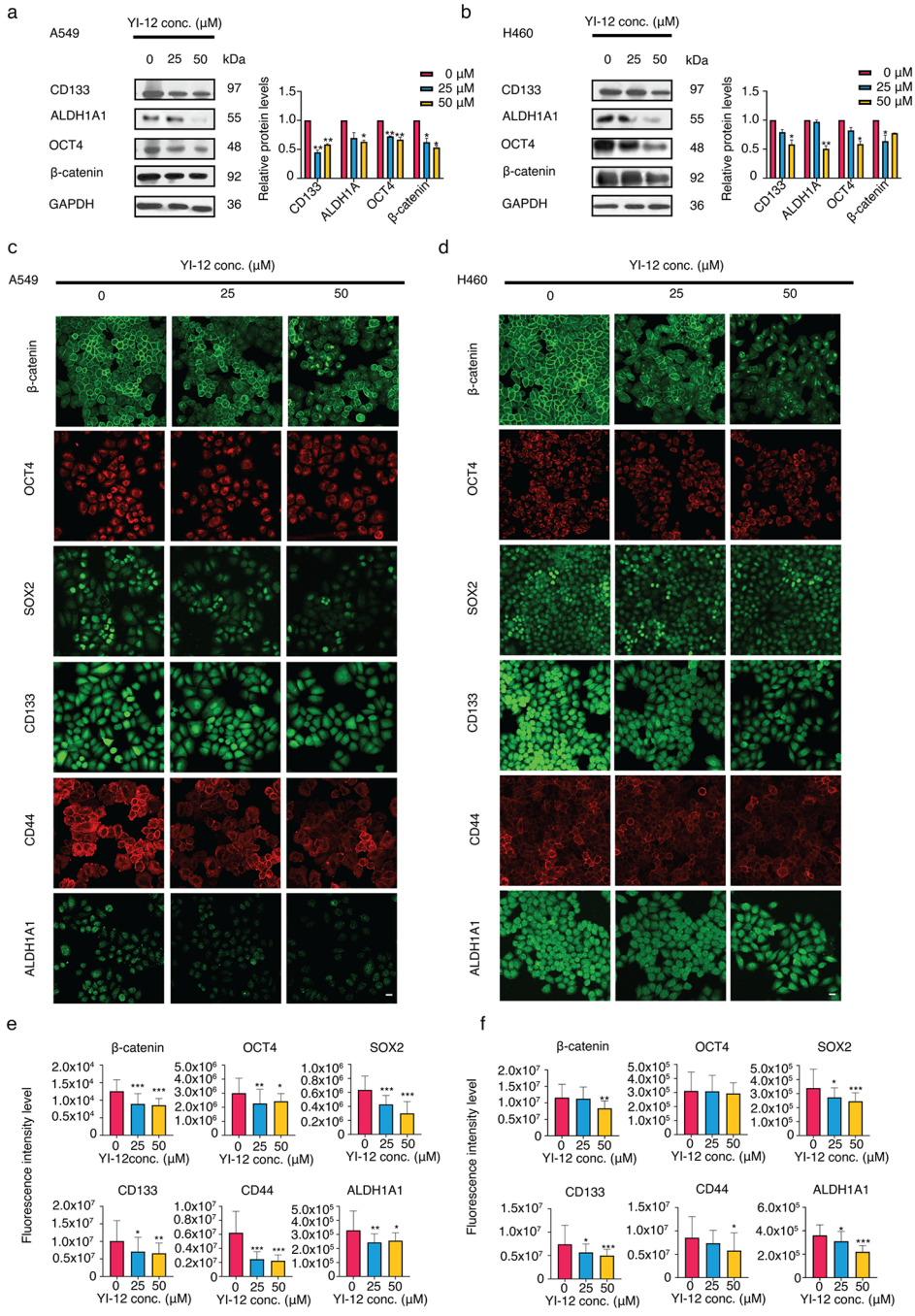

Figure 3. Effects of YI-12 on the expression levels of stem cell-related proteins, stem cell markers, and stem cell transcription factors. (a, b) Cells were treated with YI-12 (0−50 μM) for 24 h, and the protein expression levels of stem cell-related proteins (β-catenin), stem cell markers (CD133 and ALDH1A1), and stem cell transcription factors (OCT4) were determined by Western blot analysis. The blot was reprobed with GAPDH to confirm equal protein loading. (c−f) Fluorescence intensity of stem-cell-related proteins (β-catenin), stem cell markers (CD133, CD44, and ALDH1A1), and stem cell transcription factors (OCT4 and SOX2) was captured using a fluorescence microscope and quantified with ImageJ software. Data are presented as mean ± SD (n = 3). Significance is indicated as * p < 0.05, ** p < 0.01, and *** p < 0.001 versus nontreated control cells.

A549 and H460. Additionally, when compared to RES, which has IC_{50} values of 176.1 ± 9.64 μM and >200 μM for A549 and H460 cells, respectively. Therefore, YI-12 demonstrated superior efficacy compared to other RES derivatives (Figure 2a).

To assess the cancer selectivity of YI-12, experiments were conducted using the nontumorigenic human bronchial epithelial cell line (BEAS-2B). Following treatment with YI-12, the IC_{50} value for BEAS-2B was determined to be 128.5 ± 12.89 μM (Figure 2a), whereas for RES, the IC_{50} value was measured at 145.9 ± 15.55 μM. These results suggest that YI-12 has comparable toxicity to resveratrol against normal epithelial cells. Additionally, the selectivity index (SI) values of BEAS-2B cells treated with YI-12 were calculated to be 1.33 and 1.19 for A549 and H460 lung cancer cells, respectively. A selectivity index greater than 1.0 indicates preferential efficacy against tumor cells over normal cells[42] (Figure 2a).

https://doi.org/10.1021/acs.chemrestox.4c00436
Chem. Res. Toxicol. 2025, 38, 415−432

Structure−activity relationship (SAR) analysis is a widely adopted approach for predicting the biological activity of compounds based on their molecular structure in drug design and discovery. SAR aids in the synthesis of compounds by optimizing potency, minimizing toxicity, and enhancing bioavailability.[43] When the structures of the four compounds were compared, several key differences were found when compared to RES. YI-1 and YI-3, with the substitution of a hydroxyl group (OH) by a methoxymethyl ether group (OMOM), show that this modification does not significantly affect the efficacy, similar to the addition of single or double bonds in the structure. Furthermore, the incorporation of a carbonyl group within the structure, as seen in YI-10, did not enhance the biological efficacy of the compound. However, it was observed that modifying the RES structure by extending the carbon chain length and adding an O-benzyl group resulted in improved cytotoxicity.

Apoptosis was evaluated using Hoechst 33342 nuclear staining. Apoptotic cells are indicated by the presence of condensed nuclei or fragmented chromatin stained by the bright blue fluorescence of Hoechst 33342 dye. Co-staining with PI could detect accidental necrotic dead cells. Upon treatment with 0−50 μM YI-12 for 24 h, lung cancer cells (A549 and H460) exhibited varying degrees of apoptosis induction. Specifically, YI-12 treatment led to higher percentages of apoptotic cells in both cell lines compared to the nontreated control cells. The percentages of apoptotic cells were 0.85 ± 0.07 and 0.39 ± 0.18% at 0 μM, 4.20 ± 0.89 (p < 0.05) and 5.81 ± 1.55% (p < 0.01) at 25 μM, and 6.38 ± 1.62 (p < 0.01) and 11.37 ± 2.00% (p < 0.001) at 50 μM for A549 and H460, respectively (Figure 2b,c).

Furthermore, YI-12-treated lung cancer cells exhibited increased PI staining, indicating a higher number of necrotic cell deaths. The percentages of necrotic cells were 0.09 ± 0.01 and 0.09 ± 0.16% at 0 μM, 0.32 ± 0.34 and 1.28 ± 0.10% (p < 0.01) at 25 μM, and 1.36 ± 0.41 (p < 0.05) and 1.62 ± 0.49% (p < 0.01) at 50 μM for A549 and H460, respectively (Figure 2b,c). As a result, YI-12 was selected for further investigation.

YI-12 Inhibits the Proliferation and Decreases the Colony Formation. The antiproliferative effect of YI-12 was examined in NSCLC cells ranging from 0 to 50 μM. Lung cancer cells were cultured in a growth medium with or without YI-12 for 72 h, and cell viability was assessed every 24 h. The proliferation assay demonstrated that after 48 h of treatment with YI-12, the proliferation rate in H460 cells was significantly reduced at 50 μM (p < 0.01). After 72 h of YI-12 treatment, the proliferation rate in A549 cells was also significantly inhibited at 50 μM (p < 0.01). Interestingly, in H460 cells, proliferation was inhibited at both 25 μM (p < 0.05) and 50 μM (p < 0.01) (Figure s21). Thus, the proliferation rate of lung cancer cells treated with YI-12 significantly diminished in a dose-dependent manner, particularly at a concentration of 50 μM, starting at 72 h for A549 and 48 h for H460.

The colony formation assay serves as a widely used method for assessing an individual cell's ability to form colonies, specifically focusing on growth cancer cells. Following a 48 h treatment with YI-12 (at concentrations of 0, 25, and 50, μM) on NSCLC A549 and H460 cells, YI-12 was subsequently removed, and the cells were permitted to undergo colony growth for an additional 7 days (Figure 2d). The colony formation, as indicated by crystal violet staining, exhibited a markedly lower number of colonies at 25.88 ± 3.77% for H460 cells treated with 50 μM YI-12 compared to 100% for control (p < 0.001). The A549 cells treated with YI-12 showed a greater suppression in the percentage of colony formation at 7.16 ± 3.61% (p < 0.001), when exposed to 50 μM YI-12 compared to control (Figure 2e). Additionally, the colony area of both cell types significantly decreased upon treatment with YI-12 at concentrations of 25 and 50 μM (p < 0.001), as illustrated by the distribution shown in the Violin plot (Figure 2f). In summary, YI-12 significantly suppressed colony formation across all cell lines compared to the control, as illustrated in Figure 2d.

YI-12 Inhibits Stem Cell-like Properties in Human Lung Cancer Cell Lines. Cancer stem cells (CSCs) lead to tumorigenicity, progression, and resistance to treatment. Cell surface markers, such as CD44 and CD133 are commonly used to identify CSCs. CD133, in particular, is a key CSCs marker for lung cancer.[11] CD133-positive cancer cells possess self-renewal properties and the ability to generate new tumors, while CD133-negative cancer cells lack these capabilities.[44] OCT4 is a crucial transcription factor present in both CSCs and normal stem cells as it plays a key role in regulating embryogenesis and pluripotency. In CSCs, OCT4 is overexpressed and contributes to drug resistance.[45] ALDH1A1 is a key component of ALDH1, which is prominently expressed in CSCs but has low expression in normal cells. ALDH1 is involved in maintaining CSC characteristics, altering metabolism, promoting DNA repair, and driving tumor metastasis.[46] β-catenin is a key protein in the Wnt signaling pathway, which regulates the development of CSCs. During their self-renewal process, stem cells depend on β-catenin to respond to Wnt signals, which are crucial for maintaining and transitioning from a pluripotent state.[8,47] Additionally, inhibiting β-catenin has been shown to reduce stem cell markers in lung cancer cells.[15]

After 24 h of treatment with YI-12 (0−50 μM), Western blot analysis was performed to examine the levels of cancer stem cell-related proteins, including CD133, OCT4, ALDH1A, and β-catenin in A549 and H460 cells. The results showed that in A549 cells, CD133 significantly decreased by approximately 2-fold at both 25 μM and 50 μM (p < 0.01). The self-renewal protein ALDH1A significantly decreased by approximately 1.5-fold at 50 μM (p < 0.05), similar to OCT4, which also decreased by 1.5-fold (p < 0.01). Interestingly, β-catenin significantly decreased by 1.6 and 1.8-fold at 25 μM (p < 0.05) and 50 μM (p < 0.05), respectively (Figure 3a). In H460 cells, CD133 expression decreased by 1.2-fold at 25 μM and significantly decreased by 1.7-fold at 50 μM (p < 0.05). ALDH1A expression was reduced by 2-fold at 50 μM (p < 0.01). OCT4 decreased by 1.5-fold at 50 μM (p < 0.05). In contrast, β-catenin levels decreased by 1.5-fold at 25 μM (p < 0.05) (Figure 3b).

To further investigate the suppression of cancer stem cells, A549 and H460 cell lines were treated with YI-12. The expression levels of stem cell markers (CD133, CD44, and ALDH1A1) and stem cell transcription factors (OCT4 and SOX2) were analyzed by using immunofluorescence assays. The results indicated that YI-12 treatment significantly reduced the levels of stem cell markers and transcription factors in A549 cells (Figure 3c,e) and slightly reduced spheroid marker in H460 cells (Figure 3d,f). Notably, following treatment, β-catenin showed a significant reduction in the level of A549. showed a significant reduction in the number of A549 cells. Additionally, imaging analysis revealed substantial clustering near the nucleus in H460 cells treated

https://doi.org/10.1021/acs.chemrestox.4c00436
Chem. Res. Toxicol. 2025, 38, 415−432

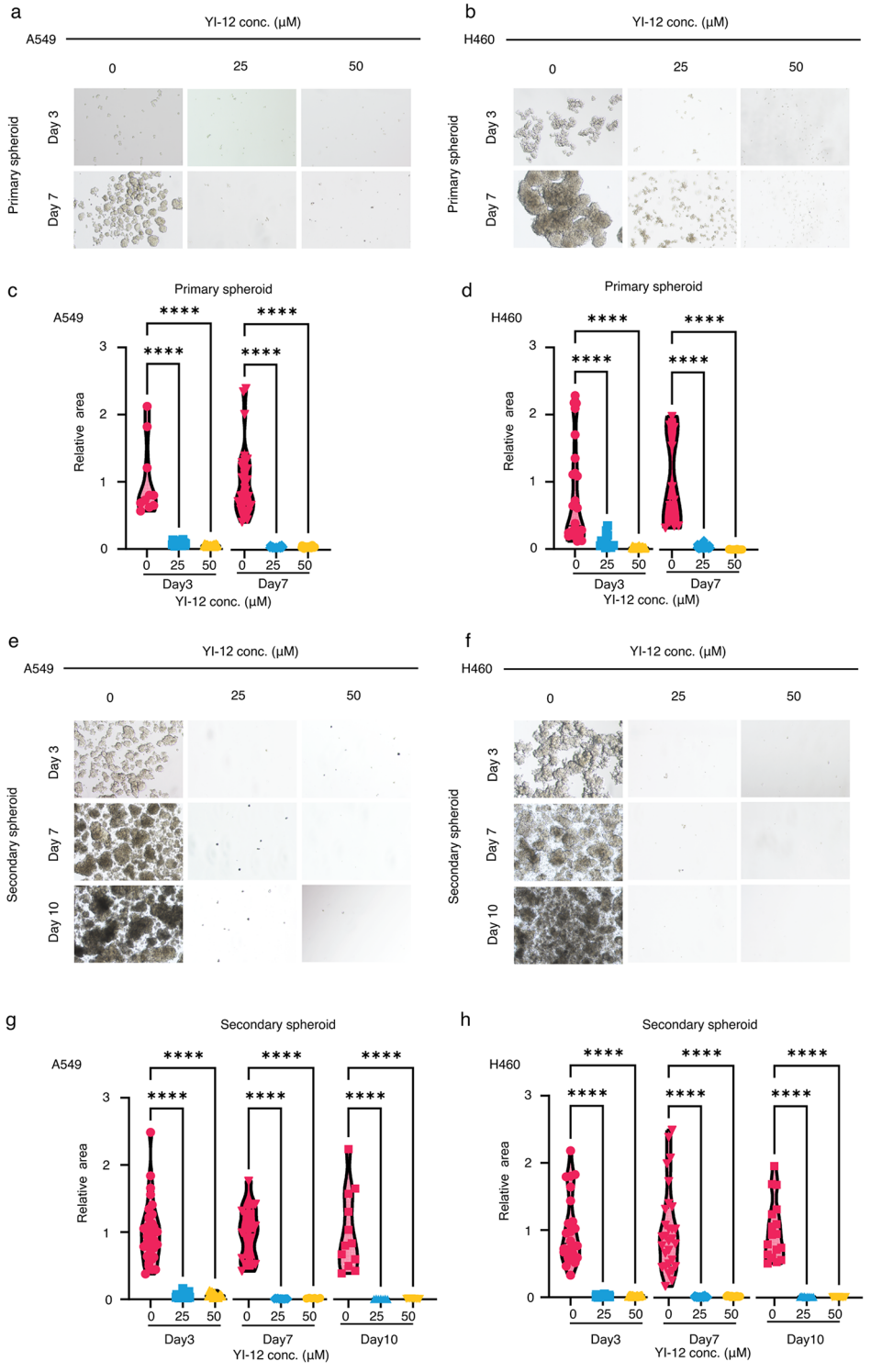

Figure 4. YI-12 suppresses cancer stem cell-like phenotypes in A549 and H460 cells. (a, e) A549 and (b, f) H460 cells were treated with YI-12 (0–50 μM) and allowed to form primary spheroids for 7 days. Primary tumor spheroids were imaged after 3 and 7 days using a phase-contrast microscope. These primary spheroids were then seeded and incubated for 10 days to form secondary CSC-enriched spheroids, with images captured on days 3, 7, and 10. The relative areas of (c, d) primary and (g, h) secondary spheroids were measured. Data are presented as mean ± SD (n = 3). Significance is indicated as **** $p < 0.0001$ versus nontreated control cells.

with 50 μM. The downregulation of these stemness markers suggests that YI-12 treatment could potentially inhibit the self-renewal and tumorigenicity of lung cancer stem-like cells. These findings imply that YI-12 might have therapeutic potential as an anticancer agent in NSCLC.

YI-12 Suppresses Cancer Stem Cell Spheroid Formation in Human Lung Cancer Cell Line. After investigating a two-dimensional (2D) cell culture model, we assessed the ability of YI-12 to inhibit CSC-like phenotypes in NSCLC by using a three-dimensional (3D) tumor spheroid formation assay. A549 and H460 cells were first treated with

https://doi.org/10.1021/acs.chemrestox.4c00436
Chem. Res. Toxicol. 2025, 38, 415–432

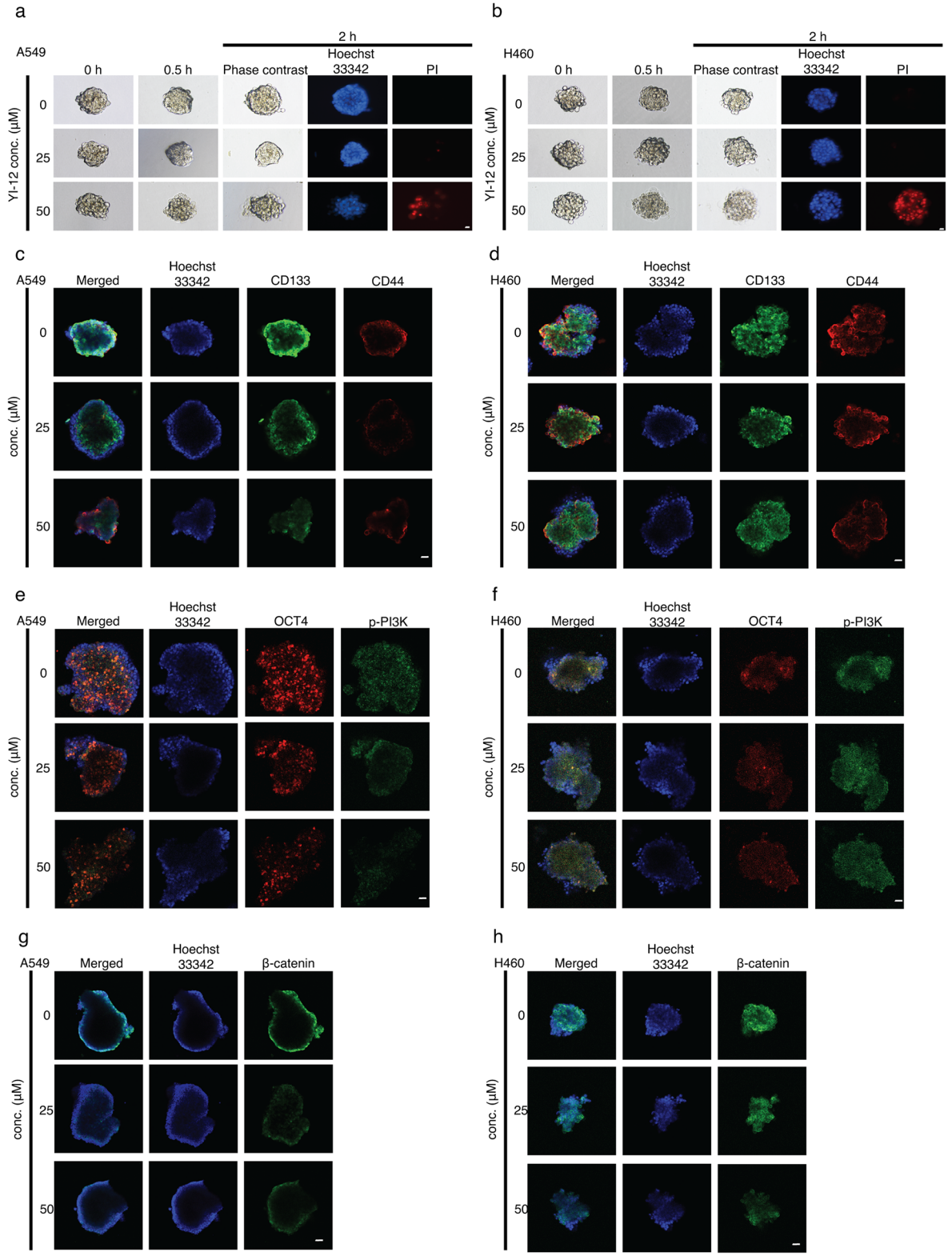

Figure 5. YI-12 induces apoptosis in CSC-rich populations of A549 and H460 cells. (a) A549 and (b) H460 cells: Single CSC-rich secondary spheroids were exposed to YI-12 (0−50 μM) for 0.5 and 2 h. Phase-contrast images of these spheroids and nontreated control cells were captured. At 2 h, a single spheroid was stained with Hoechst 33342/PI. Immunofluorescence staining of (c, e, g) A549 and (d, f, h) H460 cells was performed to assess the levels and distributions of CD133, CD44, OCT4, β-catenin, and p-PI3K. The cell nuclei were stained with Hoechst 33342, while CD44 and OCT4 were specifically labeled with an Alexa Fluor 488-labeled secondary antibody. Additionally, CD133, β-catenin, and p-PI3K were stained using an Alexa Fluor 594-labeled secondary antibody. Scale bar: 100 μm.

YI-12 (0−50 μM) for 24 h. Subsequently, the cells were cultured at a low density to form first-generation spheres over 7 days. Secondary spheroids were then formed from single cells derived from primary spheroids over 10 days.

https://doi.org/10.1021/acs.chemrestox.4c00436
Chem. Res. Toxicol. 2025, 38, 415−432

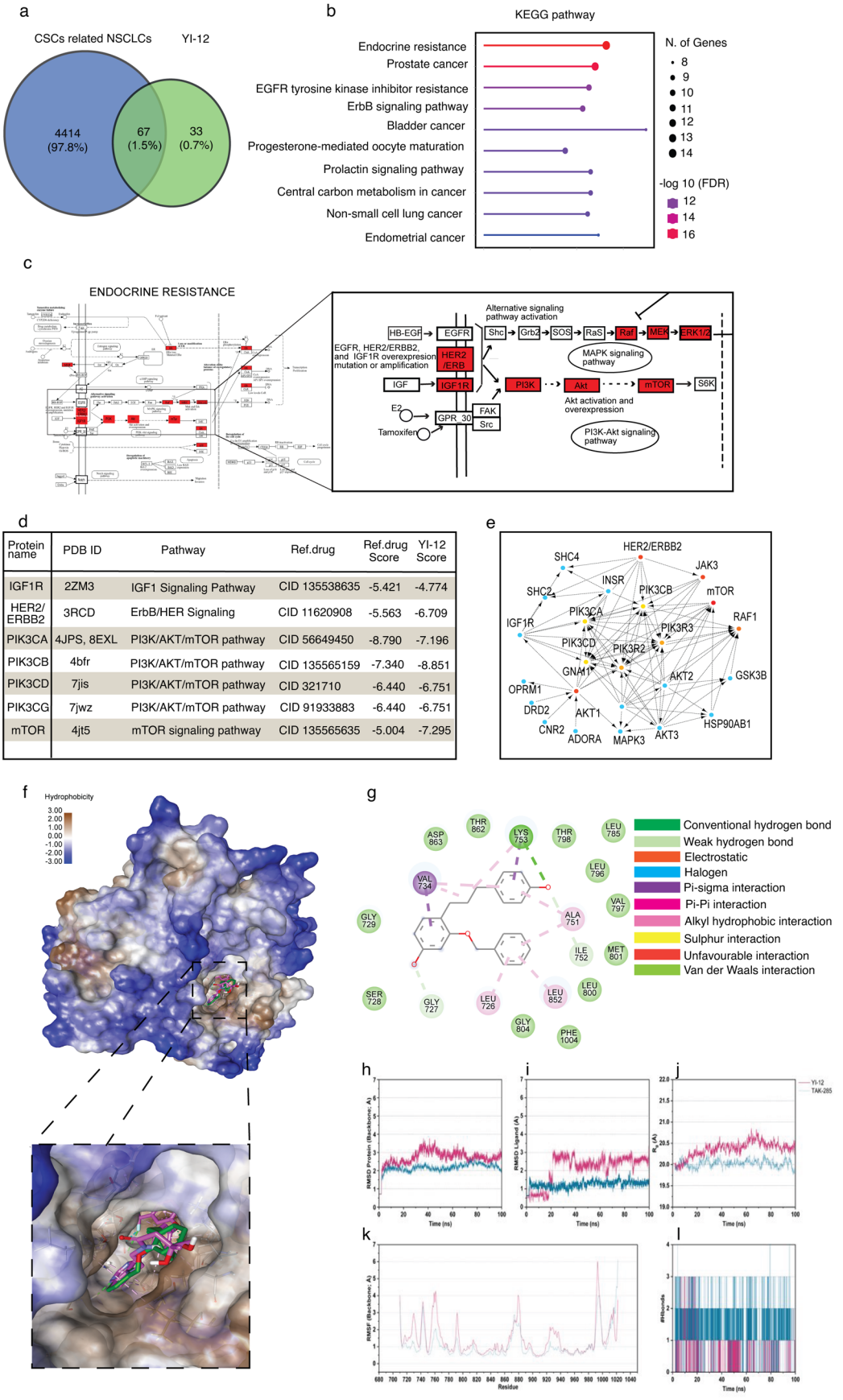

Protein name	PDB ID	Pathway	Ref.drug	Ref.drug Score	YI-12 Score
IGF1R	2ZM3	IGF1 Signaling Pathway	CID 135538635	-5.421	-4.774
HER2/ ERBB2	3RCD	ErbB/HER Signaling	CID 11620908	-5.563	-6.709
PIK3CA	4JPS, 8EXL	PI3K/AKT/mTOR pathway	CID 56649450	-8.790	-7.196
PIK3CB	4bfr	PI3K/AKT/mTOR pathway	CID 135565159	-7.340	-8.851
PIK3CD	7jis	PI3K/AKT/mTOR pathway	CID 321710	-6.440	-6.751
PIK3CG	7jwz	PI3K/AKT/mTOR pathway	CID 91933883	-6.440	-6.751
mTOR	4jt5	mTOR signaling pathway	CID 135565635	-5.004	-7.295

Figure 6. Venn diagram of the potential anti-NSCLC/CSC targets of YI-12 and KEGG analysis. (a) Venn diagram illustrating the overlap between NSCLC-related CSC targets and YI-12 targets. (b) KEGG pathway analysis was conducted with an FDR cutoff of 0.05. In this analysis, the *y*-axis represents a biological network, and the *x*-axis indicates the number of genes enriched in each term. The color gradient from blue to red represents

https://doi.org/10.1021/acs.chemrestox.4c00436
Chem. Res. Toxicol. 2025, 38, 415−432

Figure 6. continued

the p-value, with smaller FDR values indicating higher credibility and significance. (c) Endocrine resistance was found to be enriched in 14 genes: PIK3CA, BRAF, ERBB2, AKT1, mTOR, ARAF, ESR1, ESR2, MAP2K1, RAF, IGF1R, MMP9, MMP2, MAPK14, and MAPK3. (d) Binding affinities of YI-12 to its target proteins were compared to a reference compound. (e) Among the 14 targets, the potential targets were ranked based on their degree of interaction, visualized using the CytoHubba plugin. The ErbB2/HER2 (PDB ID 3RCD) interaction with the reference molecule (TAK-285; green) and YI-12 (pink). (f) Hydrophobicity surface map of ErbB2 shows that the reference molecule and YI-12 occupy the hydrophobic pocket of the protein, which is also the ATP-binding pocket of the protein. (g) YI-12, the 2D interaction diagram shows that YI-12 interacts with some of the key residues quite similar to the reference molecule (TAK-285). Graphical results from the molecular dynamics simulation of the ErBb2 − YI-12 complex, showing (h) RMSD of the protein backbone, (i) ligand RMSD, (j) radius of gyration, (k) RMSF per residue, and (l) the number of hydrogen bonds between the ligand and protein.

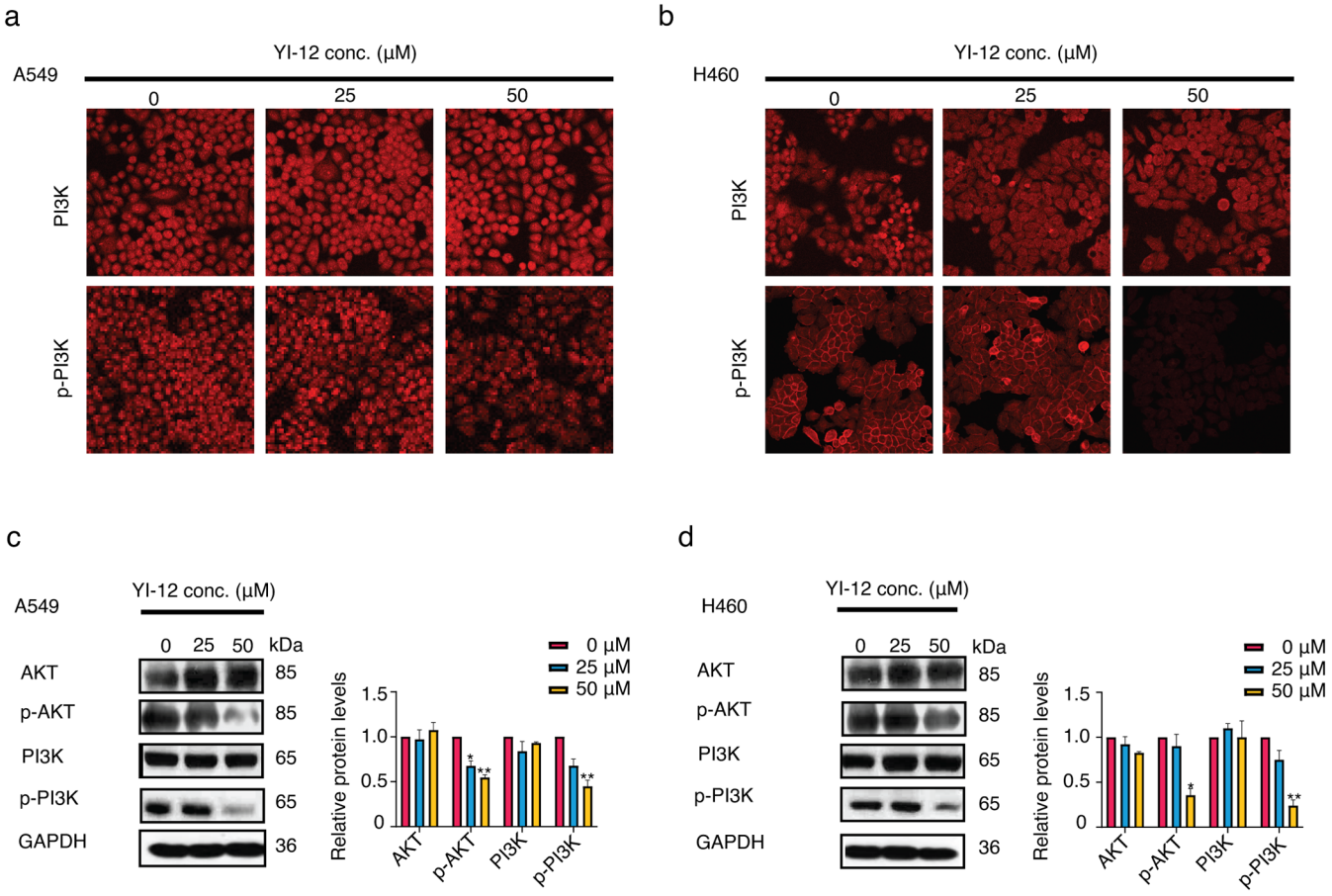

Figure 7. Effects of YI-12 on the protein levels downstream regulated by ErbB2. (a, b) Cells were treated with YI-12 (0−50 μM) for 24 h, and the protein expression levels of PI3K, p-PI3K were determined by fluorescence microscope. (c, d) Protein expression levels of PI3K, p-PI3K, AKT, and p-AKT determined by Western blot analysis. Data are presented as mean ± SD (n = 3). Significance is indicated as * $p < 0.05$, ** $p < 0.01$, and *** $p < 0.001$ versus untreated control cells.

The results showed that control cells had a high capacity for tumor spheroid formation, while cells treated with YI-12 exhibited a decreased ability to form these spheroids (Figure 4a,b,e,f). This suggests that YI-12 had a suppressive effect on the CSC populations in these cells. Specifically, at 25 ($p <$ 0.0001) and 50 μM ($p < 0.0001$), YI-12 significantly reduced the number and size of both primary and secondary spheroids compared to the control in both A549 (Figure 4c,g) and H460 cells (Figure 4d,h).

After 10 days, secondary spheroids from A549 and H460 cells, which had comparable dimensions and shapes, were selected for further treatment. These spheroids were treated with 0−50 μM YI-12, and their responses were monitored at 0, 1.5, and 2 h. Individual CSC spheroids were visible in both the control and YI-12-treated cells at these time points. At 50 μM, YI-12 treatment significantly inhibited the CSC populations and increased the death of CSC spheres in both cell lines (Figure 5a,b).

Furthermore, YI-12 reduced the expression of CSC markers, such as CD44 and CD133 (Figure 5c,d), and significantly inhibited the expression of OCT4, p-PI3k (Figure 5e,f), and β-catenin (Figure 5g,h), in CSC spheroids of both A549 and H460 cells. These findings suggest that YI-12 effectively suppresses the CSC-like properties of NSCLC cells under 3D culture conditions.

YI-12 Suppresses Human Lung CSCs via the ErbB2-Downregulated PI3K/AKT Pathway. To investigate the properties of YI-12 on NSCLC target genes, gene enrichment analysis was performed for YI-12-target genes and NSCLC target genes. In this study, we focused on genes associated with

https://doi.org/10.1021/acs.chemrestox.4c00436
Chem. Res. Toxicol. 2025, 38, 415−432

cancer stem cells in NSCLCs. As shown in the Venn diagram in Figure 6a, the 4481 genes were identified as targets of NSCLCs/CSCs, and 100 genes were identified as targets of YI-12. There are 67 intersecting genes that were obtained as potential anti-NSCLC/CSC targets.

To explore the biological functions of the 67 target genes, KEGG pathway analyses were performed with an FDR cutoff of 0.05. According to KEGG pathway analysis, the network was involved in "Endocrine resistance", "Prostate cancer", "EGFR tyrosine kinase inhibitor resistance", "ErbB signaling pathway", and "Bladder cancer", "Progesterone-mediated oocyte maturation", Prolactin signaling pathway", Central carbon metabolism in cancer", "non-small-cell lung cancer", Endometrial cancer" (Figure 6b). The first pathway, Endocrine resistance (Figure 6c), was enriched for 14 genes, namely, PIK3CA, BRAF, ErbB2, AKT1, mTOR, ARAF, ESR1, ESR2, MAP2K1, RAF, IGF1R, MMP9, MMP2, MAPK14, and MAPK3. Interestingly, 5 out of the 14 target genes, IGF1R, ERBB2, PIK3 AKT1, mTOR were mainly involved in PI3K-AKT signaling pathway. Therefore, the 4 gene targets were selected to compare with reference compound for molecular docking with 7compounds, namely, CID135538635, CID11620908, CID56649450, CID135565159, CID321710, CID91933883, and CID135565638. In comparison to reference drugs, YI-12 (Figure 6d) showed better interactions with HER2/ERBB2, PIK3CB, and mTOR and had docking scores of −6.709, −8.851, and −7.295 kcal/mol, respectively.

To confirm the potential for further target identification, protein−protein interactions were performed. The top 10 hub genes were evaluated by the DMNM method and are shown in Figure 6e. The network analysis revealed mTOR, HER2/ErbB2, JAK3, GNAI1, PIK3R2, PIK3R3, PIK3CA, PIK3CD, PIK3CB, and GSK3A as the top key targets.

The functional enrichment analysis showed that the 67 key targets were enriched in various signaling pathways, including the "PI3K-AKT signaling pathway"; therefore, expression levels of PI3K and AKT protein were performed to verify the effect of YI-12 on these targets and pathways (Figure 7).

Binding Interaction of YI-12 with ErbB2. The further analysis of ErbB2-ligand docking focused on their interactions. Figure 6f shows that both YI-12 and TAK-285 (as the reference molecule) occupy the same hydrophobic pocket in ErbB2, which is also the ATP-binding pocket of the protein. This pocket is crucial for the kinase activity of ErbB2, as it binds ATP, facilitating phosphorylation events that drive signal transduction pathways.[48] However, due to differences in length and structural geometry between TAK-285 and YI-12, their overall interactions are not identical. TAK-285 has a less bent geometry, allowing it to adopt a suitable conformation to occupy the deep lipophilic pocket of ErbB2. In contrast, YI-12, due to its substituted meta-dihydroxyl side group, exhibits a more bent geometry.

The 2D interaction diagram (Figures 6g and S25) shows that TAK-285 uses its 3-hydroxy-3-methylbutanamide substituent to interact with Gly727, a residue located near the opening of the hydrophobic pocket of ErbB2. Meanwhile, YI-12 interacts with Gly727 through its 4-hydroxyl group on the benzyl-substituted moiety. In accordance with the reported crystallized structure,[49] the redocking of TAK-285 to ErbB2 shows that its 4-anilino group interacts with residues in the back lipophilic pocket of the ATP-binding pocket of ErbB2, notably with Phe864 of ErbB2's DFG motif. This interaction is significant as the DFG motif is involved in the activation of the kinase domain.[50]

In contrast, YI-12 does not interact directly with the DFG motif but still engages with residues in the deep lipophilic pocket such as Val734, Ala751, and Lys753, which also interact with TAK-285. The lack of hydrogen bond acceptors or donors in YI-12, compared to TAK-285, results in fewer hydrogen bond interactions between the molecule and the protein. However, since the docking score of YI-12 is more negative than that of TAK-285, it appears that the hydrophobic interaction between YI-12 and the ATP-binding pocket is more favorable. These findings suggest that YI-12 might induce a different conformational change in ErbB2, potentially leading to altered inhibitory effects. This information could be valuable for the design of new inhibitors targeting the ATP-binding pocket of ErbB2, offering insight into the structural requirements for effective binding and inhibition.

Molecular dynamics simulations were performed on the ErbB2 − YI-12 complex to evaluate the stability of the interaction. The results of the simulation are presented in Figure 6h,l. The RMSD of the protein backbone increases up to 20 ns, after which it stabilizes, suggesting initial structural rearrangements before reaching a relatively stable conformation. Beyond 20 ns, the RMSD remains between 2.5 and 3.5 Å, indicating that the protein maintains a consistent structure with only minor deviations in backbone conformation. The radius of gyration (R_g) remains stable between 20 and 21 Å, indicating that the protein retains its compact structure throughout the simulation (Figure 6j).

The RMSF per residue highlights that the region contributing most to the conformational changes is the random coil near the C-terminus of ErbB2. Importantly, the DFG motif remains in the DFG-in conformation, which is typically associated with the active state of kinases,[51] suggesting that YI-12 inhibits the active form of ErbB2 rather than stabilizing its inactive form, similar to TAK-285.[49]

The ligand RMSD (Figure 6i) shows an increase around 20 ns, stabilizing after 22 ns. Analysis of the trajectory reveals that this conformational change is due to the flipping of the carbon chain penetrating the hydrophobic pocket of ErbB2, which reorients the resorcinol bridge of YI-12 (Figure S24). Despite this shift, the ligand remains in the binding pocket after 100 ns, with no indication of dissociation. The number of hydrogen bonds between the ligand and protein fluctuates, averaging 1−2 bonds over the simulation. The solvated interaction energy, calculated over the last 15 ns of the simulation, was −8.05 ± 0.37 kcal/mol, indicating a moderately stable binding affinity between the ligand and the protein. Given the limited number of hydrogen bonds, hydrophobic interactions likely play a dominant role in stabilizing the protein−ligand interaction (Figure 6k,l).

Previous studies have demonstrated that inhibitors targeting ErbB2/HER2 can reduce the phosphorylation of PI3K and AKT.[21,52] In this study, we investigated the downstream proteins of ErbB2, specifically PI3K and AKT. Our findings revealed that p-PI3K expression significantly decreased in both A549 and H460 cells following 50 μM YI-12 treatment (Figure 7a,b). Furthermore, Western blot analysis confirmed the reduction in the levels of p-PI3K and AKT (Figure 7c,d).

DISCUSSION

In the next decade, it is anticipated that up to 40% of people will suffer from lung cancer. Unfortunately, the success rate of

https://doi.org/10.1021/acs.chemrestox.4c00436
Chem. Res. Toxicol. 2025, 38, 415−432

treatment remains low due to resistance to chemotherapy. There is an urgent need for novel therapeutic compounds. CSCs are a specialized group of cancer cells with enhanced abilities for self-renewal and differentiation into various cell types. It has been reported that CSCs are responsible for driving aggressive cancer behaviors and resisting chemotherapy.[7] RES is a well-known compound derived from natural sources with anticancer properties, as a potential agent for targeting CSCs. Evidence supports that RES exhibits anticancer properties. For instance, it has been shown to be effective against human carcinomas, including bladder (RT4, T24), breast (SW620), colon (HT29), and lung (A549, H460) cancer cells.[53−57] Several reports have suggested that many RES derivatives, such as moscatilin and pterostilbene, have the ability to inhibit CSCs.[9,13] Therefore, this study modifying the chemical structure of RES to create RES analogue YI-12, has been found to enhance the suppression of CSCs such as CD133, ALDH1A1, and OCT4. Our results showed that YI-12 is more effective in suppressing the viability of lung cancer cells compared to RES (Figure 2a). Furthermore, YI-12 effectively inhibits colony formation, as demonstrated by a significant reduction in cell numbers at 25 and 50 μM. These findings align with previous studies on RES analogues in pancreatic cancer cells, which reported a decrease in cell numbers after 72 h of treatment.[58] Notably, our study also observed a significant reduction in cell size in addition to the reduction in cell numbers. Additionally, nuclear staining results confirm that the highest concentration used did not cause immediate necrosis after treatment. Thus, YI-12 effectively reduces cell viability in lung cancer cell lines A549 and H460, with an IC_{50} of less than 100 μM, lower than the IC_{50} of RES, suggesting that YI-12 could be a promising anticancer agent for treating lung cancer. Moreover, YI-12 demonstrates low toxicity to normal cells (Figure 2b), indicating a selective therapeutic index (Figure 2c).

Various treatment strategies have been investigated for NSCLCs, with a particular focus on targeting CSCs and modulating self-renewal pathways as a central approach in lung cancer therapy.[8,9] There is also evidence that the process of self-renewal and the overexpression of CSCs transcriptional factors contribute to drug resistance and invasion in cancer cells, making treatment more challenging.[5] Therefore, three-dimensional spheroids, which simulate cancer cells in vivo, are an effective method for in vitro drug screening and led to the discovery of new anticancer compounds.[59,60] Additionally, the formation of spheroids is associated with a significant increase in the expression of stem cell markers (CD133, CD44, and ALDH1A1) and stem cell transcription factors (OCT4 and SOX2), which plays a crucial role in the self-renewal and proliferation of these spheroids.[12] In our experiment, we observed that stemness markers, including CD133, CD44, ALDH1A1, and OCT4, were downregulated following treatment with YI-12 in both A549 and H460 cells. Additionally, the CSCs-related protein β-catenin, which regulates these markers, was also diminished (Figures 3 and 5). Furthermore, our study on spheroid formation inhibition demonstrated that YI-12 could effectively inhibit spheroid formation starting from day 3 of the experiment in both cell lines (Figure 4). Therefore, the YI-12 compound shows promise as a targeted treatment for CSC-rich subpopulations in lung cancer.

The human epidermal growth receptor (HER) family, also known as ErbB, consists of a group of proteins that function as receptors on the cell membrane with tyrosine kinase activity.[19,22,61] This family includes HER1, HER2, HER3, and HER4. HER1 is commonly known as EGFR. ErbB2/HER2 is a proto-oncogene located on the long arm of chromosome 17.[61] HER2 normally forms homodimers or heterodimers with other HER proteins and is involved in signaling to other proteins such as the PI3K/AKT pathway and the RAS/RAF/MEK/ERK pathway, which influence cell proliferation processes.[18,21,52] Additionally, PI3K and AKT are crucial proteins responsible for regulating CSCs.[62,63] Moreover, PI3K/AKT signaling stimulates the activation of CD133/p85 interaction, which is associated with tumorigenicity in cancer cells.[64] Based on the results from immunofluorescence and Western blot analysis, it was found that treatment with YI-12 in human lung cancer cells led to a reduction in proteins regulated by the ERBB2/HER2 pathway, specifically PI3K and AKT. Our findings indicate that the decrease in p-PI3K levels in both adherent (monolayer) cells and CSC-rich spheroids (Figures 3, 5, and 7) is a direct result of YI-12 treatment. Thus, we can connect the dots that the reduction in PI3K signaling is due to the suppression of ErbB2 receptor activity. Similar to previous research by Son et al., it was observed that p-AKT levels decreased following the inhibition of ErbB2/HER2 after treatment.[52] This inhibition consequently leads to a decrease in the number of proteins associated with CSCs, including β-catenin, OCT4, SOX2, CD133, CD44, and ALDH1A1 (Figure 3). Additionally, molecular docking studies have shown that the RES analogue YI-12 binds effectively to the binding site of ErbB2, compared to the reference compound TAK-285 (Figures 6 and 7).

CONCLUSIONS

we have uncovered the anticancer activity of RES-modified analogue YI-12 against CSCs in lung cancer cells. YI-12 was found to be more potent than its parent compound in terms of both cytotoxicity and selectivity. Our research demonstrated that YI-12 suppresses human lung CSCs via the ErbB2-downregulated PI3K/AKT pathway. Furthermore, molecular docking revealed that YI-12 interacts with the ErbB2 receptor, showing a greater binding affinity to the ErbB2 binding pocket compared with the reference compound. These findings highlight the potential of YI-12 as an alternative therapeutic agent for targeting lung CSCs through the ErbB2 receptor. Overall, this research paves the way for future studies and clinical development of this compound.

ASSOCIATED CONTENT

Supporting Information

The Supporting Information is available free of charge at https://pubs.acs.org/doi/10.1021/acs.chemrestox.4c00436.

1H NMR spectra for all compounds (Figures S1−S21); proliferative effect of YI-12 on lung cancer cells was evaluated by MTT assay at 24, 48, and 72 h (Figure S22); superimposed structure of ref Drug and YI-12 (Figure S23); validation of the docking protocol (Table S2); characteristics of YI-12 and reference drugs (Tables S3−S8); snapshot from the molecular dynamic trajectory illustrating the conformational change of YI-12 (Figure S24); ErbB2/HER2 (PDB ID 3RCD) interaction with the reference molecule (TAK-285; green) (Figure S25); and RES as positive control for all in vivo experiments (Figures S26−S29) (PDF)

https://doi.org/10.1021/acs.chemrestox.4c00436
Chem. Res. Toxicol. 2025, 38, 415−432

AUTHOR INFORMATION

Corresponding Author

Pithi Chanvorachote − *Department of Pharmacology and Physiology, Faculty of Pharmaceutical Sciences, Chulalongkorn University, Bangkok 10330, Thailand; Center of Excellence in Cancer Cell and Molecular Biology, Faculty of Pharmaceutical Sciences, Chulalongkorn University, Bangkok 10330, Thailand;* orcid.org/0000-0002-3103-3249; Email: pithi.c@chula.ac.th

Authors

Tanapon Soonthonsrima − *Department of Pharmacology and Physiology, Faculty of Pharmaceutical Sciences, Chulalongkorn University, Bangkok 10330, Thailand; Center of Excellence in Cancer Cell and Molecular Biology, Faculty of Pharmaceutical Sciences, Chulalongkorn University, Bangkok 10330, Thailand;* orcid.org/0009-0000-5080-171X

Ismail Dwi Putra − *Center of Excellence in Cancer Cell and Molecular Biology and Pharmaceutical Sciences and Technology Graduate Program, Faculty of Pharmaceutical Sciences, Chulalongkorn University, Bangkok 10330, Thailand*

Preeyaphan Phookphan − *Department of Pharmacology and Physiology, Faculty of Pharmaceutical Sciences, Chulalongkorn University, Bangkok 10330, Thailand; Center of Excellence in Cancer Cell and Molecular Biology, Faculty of Pharmaceutical Sciences, Chulalongkorn University, Bangkok 10330, Thailand*

Zin Zin Ei − *Department of Pharmacology and Physiology, Faculty of Pharmaceutical Sciences, Chulalongkorn University, Bangkok 10330, Thailand; Center of Excellence in Cancer Cell and Molecular Biology, Faculty of Pharmaceutical Sciences, Chulalongkorn University, Bangkok 10330, Thailand*

Masashi Yokoya − *Department of Pharmaceutical Chemistry, Meiji Pharmaceutical University, Kiyose, Tokyo 204-8588, Japan;* orcid.org/0000-0003-0187-7595

Complete contact information is available at: https://pubs.acs.org/10.1021/acs.chemrestox.4c00436

Author Contributions

⊥T.S., I.D.P., P.P., Z.Z.E., and P.C. contributed equally to this work. The manuscript was written through contributions of all authors. All authors have given approval to the final version of the manuscript. CRediT: **Tanapon Soonthonsrima** conceptualization, formal analysis, funding acquisition, investigation, methodology, validation, visualization, writing - original draft, writing - review & editing; **Ismail Dwi Putra** formal analysis, investigation, methodology, validation, visualization, writing - original draft; **Preeyaphan Phookphan** conceptualization, formal analysis, investigation, methodology, validation, visualization, writing - original draft; **Zin Zin Ei** formal analysis, investigation, methodology; **Masashi Yokoya** methodology, resources, validation, writing - original draft; **Pithi Chanvorachote** conceptualization, project administration, resources, supervision, validation, visualization, writing - original draft, writing - review & editing.

Funding

This project was funded by the National Research Council of Thailand (NRCT) No. N42A670567.

Notes

The authors declare no competing financial interest.
Any additional relevant notes should be placed here.

ACKNOWLEDGMENTS

T.S. is grateful to Ratchadapisek Somphot Fund for Postdoctoral Fellowship, Chulalongkorn University, for their postdoctoral fellowship, and the authors sincerely appreciate Yukiha Iida's valuable contributions to the synthesis of the compounds used in this study.

ABBREVIATIONS

CCR2, CC chemokine receptor 2; CCL2, CC chemokine ligand 2; CCR5, CC chemokine receptor 5; TLC, thin-layer chromatography

REFERENCES

(1) Deo, S. V. S.; Sharma, J.; Kumar, S. GLOBOCAN 2020 Report on Global Cancer Burden: Challenges and Opportunities for Surgical Oncologists. *Ann. Surg. Oncol.* **2022**, *29* (11), 6497−6500.

(2) Bray, F.; Laversanne, M.; Sung, H.; Ferlay, J.; Siegel, R. L.; Soerjomataram, I.; Jemal, A. Global Cancer Statistics 2022: GLOBOCAN Estimates of Incidence and Mortality Worldwide for 36 Cancers in 185 Countries. *Ca-Cancer J. Clin.* **2024**, *74* (3), 229−263.

(3) Ward, R. A.; Fawell, S.; Floc'h, N.; Flemington, V.; McKerrecher, D.; Smith, P. D. Challenges and Opportunities in Cancer Drug Resistance. *Chem. Rev.* **2021**, *121* (6), 3297−3351.

(4) Dean, M.; Fojo, T.; Bates, S. Tumour Stem Cells and Drug Resistance. *Nat. Rev. Cancer* **2005**, *5* (4), 275−284.

(5) Li, Y.; Wang, Z.; Ajani, J. A.; Song, S. Drug Resistance and Cancer Stem Cells. *Cell Commun. Signaling* **2021**, *19* (1), No. 19.

(6) Chu, X.; Tian, W.; Ning, J.; Xiao, G.; Zhou, Y.; Wang, Z.; Zhai, Z.; Tanzhu, G.; Yang, J.; Zhou, R. Cancer Stem Cells: Advances in Knowledge and Implications for Cancer Therapy. *Signal Transduction Targeted Ther.* **2024**, *9* (1), No. 170.

(7) Huang, B.; Yan, X.; Li, Y. Cancer Stem Cell for Tumor Therapy. *Cancers* **2021**, *13* (19), No. 4814.

(8) Yang, L.; Shi, P.; Zhao, G.; Xu, J.; Peng, W.; Zhang, J.; Zhang, G.; Wang, X.; Dong, Z.; Chen, F.; Cui, H. Targeting Cancer Stem Cell Pathways for Cancer Therapy. *Signal Transduction Targeted Ther.* **2020**, *5* (1), No. 8.

(9) Zhang, L.; Wen, X.; Li, M.; Li, S.; Zhao, H. Targeting Cancer Stem Cells and Signaling Pathways by Resveratrol and Pterostilbene. *BioFactors* **2018**, *44* (1), 61−68.

(10) Pospieszna, J.; Dams-Kozlowska, H.; Udomsak, W.; Murias, M.; Kucinska, M. Unmasking the Deceptive Nature of Cancer Stem Cells: The Role of CD133 in Revealing Their Secrets. *IJMS* **2023**, *24* (13), No. 10910.

(11) Tan, Y.; Chen, B.; Xu, W.; Zhao, W.; Wu, J. Clinicopathological Significance of CD133 in Lung Cancer: A Meta-Analysis. *Mol. Clin. Oncol.* **2014**, *2* (1), 111−115.

(12) Zheng, Y.; Wang, L.; Yin, L.; Yao, Z.; Tong, R.; Xue, J.; Lu, Y. Lung Cancer Stem Cell Markers as Therapeutic Targets: An Update on Signaling Pathways and Therapies. *Front. Oncol.* **2022**, *12*, No. 873994.

(13) Thongsom, S.; Racha, S.; Petsri, K.; Ei, Z. Z.; Visuttijai, K.; Moriue, S.; Yokoya, M.; Chanvorachote, P. Structural Modification of Resveratrol Analogue Exhibits Anticancer Activity against Lung Cancer Stem Cells via Suppression of Akt Signaling Pathway. *BMC Complementary Med. Ther.* **2023**, *23* (1), No. 183.

(14) Zhou, H.; Yu, C.; Kong, L.; Xu, X.; Yan, J.; Li, Y.; An, T.; Gong, L.; Gong, Y.; Zhu, H.; Zhang, H.; Yang, X.; Li, Y. B591, a Novel Specific Pan-PI3K Inhibitor, Preferentially Targets Cancer Stem Cells. *Oncogene* **2019**, *38* (18), 3371−3386.

(15) Ei, Z. Z.; Racha, S.; Yokoya, M.; Hotta, D.; Zou, H.; Chanvorachote, P. Simplified Synthesis of Renieramycin T Deriva-

tives to Target Cancer Stem Cells via β-Catenin Proteasomal Degradation in Human Lung Cancer. *Mar. Drugs* **2023**, *21* (12), No. 627.
(16) Dunn, S.; Eberlein, C.; Yu, J.; Gris-Oliver, A.; Ong, S. H.; Yelland, U.; Cureton, N.; Staniszewska, A.; McEwen, R.; Fox, M.; Pilling, J.; Hopcroft, P.; Coker, E. A.; Jaaks, P.; Garnett, M. J.; Isherwood, B.; Serra, V.; Davies, B. R.; Barry, S. T.; Lynch, J. T.; Yusa, K. AKT-mTORC1 Reactivation Is the Dominant Resistance Driver for PI3Kβ/AKT Inhibitors in PTEN-Null Breast Cancer and Can Be Overcome by Combining with Mcl-1 Inhibitors. *Oncogene* **2022**, *41* (46), 5046−5060.
(17) Reid, A.; Vidal, L.; Shaw, H.; De Bono, J. Dual Inhibition of ErbB1 (EGFR/HER1) and ErbB2 (HER2/Neu). *Eur. J. Cancer* **2007**, *43* (3), 481−489.
(18) Uy, N. F.; Merkhofer, C. M.; Baik, C. S. HER2 in Non-Small Cell Lung Cancer: A Review of Emerging Therapies. *Cancers* **2022**, *14* (17), No. 4155.
(19) Yu, Y.; Yang, Y.; Li, H.; Fan, Y. Targeting HER2 Alterations in Non-Small Cell Lung Cancer: Therapeutic Breakthrough and Challenges. *Cancer Treat. Rev.* **2023**, *114*, No. 102520.
(20) Yuan, Y.; Hao, L.; Huang, J.-S.; Zhao, F.-Y.; Ju, Y.-H.; Wang, J.-M.; Zhang, T.; Li, B.-Q.; Yu, Z.-W. Promotion of Stem Cell-like Phenotype of Lung Adenocarcinoma by FAM83A via Stabilization of ErbB2. *Cell Death Dis.* **2024**, *15* (6), No. 460.
(21) Bose, P.; Ozer, H. Neratinib: An Oral, Irreversible Dual EGFR/HER2 Inhibitor for Breast and Non-Small Cell Lung Cancer. *Expert Opin. Invest. Drugs* **2009**, *18* (11), 1735−1751.
(22) Baraibar, I.; Mezquita, L.; Gil-Bazo, I.; Planchard, D. Novel Drugs Targeting EGFR and HER2 Exon 20 Mutations in Metastatic NSCLC. *Crit. Rev. Oncol./Hematol.* **2020**, *148*, No. 102906.
(23) Bhaskara, V. K.; Mittal, B.; Mysorekar, V. V.; Amaresh, N.; Simal-Gandara, J. Resveratrol, Cancer and Cancer Stem Cells: A Review on Past to Future. *Curr. Res. Food Sci.* **2020**, *3*, 284−295.
(24) Wenzel, E.; Somoza, V. Metabolism and Bioavailability Oftrans-Resveratrol. *Mol. Nutr. Food Res.* **2005**, *49* (5), 472−481.
(25) Roberti, M.; Pizzirani, D.; Simoni, D.; Rondanin, R.; Baruchello, R.; Bonora, C.; Buscemi, F.; Grimaudo, S.; Tolomeo, M. Synthesis and Biological Evaluation of Resveratrol and Analogues as Apoptosis-Inducing Agents. *J. Med. Chem.* **2003**, *46* (16), 3546−3554.
(26) Pecyna, P.; Wargula, J.; Murias, M.; Kucinska, M. More Than Resveratrol: New Insights into Stilbene-Based Compounds. *Biomolecules* **2020**, *10* (8), No. 1111.
(27) Greer, A. K.; Madadi, N. R.; Bratton, S. M.; Eddy, S. D.; Mazerska, Z.; Hendrickson, H. P.; Crooks, P. A.; Radominska-Pandya, A. Novel Resveratrol-Based Substrates for Human Hepatic, Renal, and Intestinal UDP-Glucuronosyltransferases. *Chem. Res. Toxicol.* **2014**, *27* (4), 536−545.
(28) Innets, B.; Thongsom, S.; Petsri, K.; Racha, S.; Yokoya, M.; Moriue, S.; Chaotham, C.; Chanvorachote, P. Akt/mTOR Targeting Activity of Resveratrol Derivatives in Non-Small Lung Cancer. *Molecules* **2022**, *27* (23), No. 8268.
(29) Plourde, G. L.; Fisher, B. B. Synthesis of 6-Methoxy-1-Oxaspiro[4,5]Deca-6,9-Diene-8-One. *Molecules* **2002**, *7* (2), 315−319.
(30) Rikimaru, K.; Wakabayashi, T.; Abe, H.; Tawaraishi, T.; Imoto, H.; Yonemori, J.; Hirose, H.; Murase, K.; Matsuo, T.; Matsumoto, M.; Nomura, C.; Tsuge, H.; Arimura, N.; Kawakami, K.; Sakamoto, J.; Funami, M.; Mol, C. D.; Snell, G. P.; Bragstad, K. A.; Sang, B.-C.; Dougan, D. R.; Tanaka, T.; Katayama, N.; Horiguchi, Y.; Momose, Y. Structure−Activity Relationships and Key Structural Feature of Pyridyloxybenzene-Acylsulfonamides as New, Potent, and Selective Peroxisome Proliferator-Activated Receptor (PPAR) γ Agonists. *Bioorg. Med. Chem.* **2012**, *20* (10), 3332−3358.
(31) Gester, S.; Pietzsch, J.; Wuest, F. R. Synthesis of ^{18}F-labelled Stilbenes from 4-[^{18}F]Fluorobenz-aldehyde Using the Horner−Wadsworth−Emmons Reaction. *J. Labelled Compd. Radiopharm.* **2007**, *50* (2), 105−113.
(32) Lu, Y.; Kasahara, A.; Hyodo, T.; Ohara, K.; Yamaguchi, K.; Otani, Y.; Ohwada, T. Isolation and Reactions of Imidoyl Fluorides Generated from Oxime Using the Diethylaminosulfur Trifluoride/Tetrahydrofuran (DAST−THF) System. *Org. Lett.* **2023**, *25* (19), 3482−3486.
(33) Schindelin, J.; Arganda-Carreras, I.; Frise, E.; Kaynig, V.; Longair, M.; Pietzsch, T.; Preibisch, S.; Rueden, C.; Saalfeld, S.; Schmid, B.; Tinevez, J.-Y.; White, D. J.; Hartenstein, V.; Eliceiri, K.; Tomancak, P.; Cardona, A. Fiji: An Open-Source Platform for Biological-Image Analysis. *Nat. Methods* **2012**, *9* (7), 676−682.
(34) Thepthanee, C.; Ei, Z. Z.; Benjakul, S.; Zou, H.; Petsri, K.; Innets, B.; Chanvorachote, P. Shrimp Lipids Inhibit Migration, Epithelial−Mesenchymal Transition, and Cancer Stem Cells via Akt/mTOR/c-Myc Pathway Suppression. *Biomedicines* **2024**, *12* (4), No. 722.
(35) Ge, S. X.; Jung, D.; Yao, R. ShinyGO: A Graphical Gene-Set Enrichment Tool for Animals and Plants. *Bioinformatics* **2020**, *36* (8), 2628−2629.
(36) Wu, C.; Tong, L.; Wu, C.; Chen, D.; Chen, J.; Li, Q.; Jia, F.; Huang, Z. Two miRNA Prognostic Signatures of Head and Neck Squamous Cell Carcinoma: A Bioinformatic Analysis Based on the TCGA Dataset. *Cancer Med.* **2020**, *9* (8), 2631−2642.
(37) Trott, O.; Olson, A. J. AutoDock Vina: Improving the Speed and Accuracy of Docking with a New Scoring Function, Efficient Optimization, and Multithreading. *J. Comput. Chem.* **2010**, *31* (2), 455−461.
(38) Eberhardt, J.; Santos-Martins, D.; Tillack, A. F.; Forli, S. AutoDock Vina 1.2.0: New Docking Methods, Expanded Force Field, and Python Bindings. *J. Chem. Inf. Model.* **2021**, *61* (8), 3891−3898.
(39) Dolinsky, T. J.; Czodrowski, P.; Li, H.; Nielsen, J. E.; Jensen, J. H.; Klebe, G.; Baker, N. A. PDB2PQR: Expanding and Upgrading Automated Preparation of Biomolecular Structures for Molecular Simulations. *Nucleic Acids Res.* **2007**, *35*, W522−W525.
(40) Sulea, T.; Cui, Q.; Purisima, E. O. Solvated Interaction Energy (SIE) for Scoring Protein−Ligand Binding Affinities. 2. Benchmark in the CSAR-2010 Scoring Exercise. *J. Chem. Inf. Model.* **2011**, *51* (9), 2066−2081.
(41) Purisima, E. O.; Corbeil, C. R.; Gaudreault, F.; Wei, W.; Deprez, C.; Sulea, T. Solvated Interaction Energy: From Small-Molecule to Antibody Drug Design. *Front. Mol. Biosci.* **2023**, *10*, No. 1210576.
(42) Indrayanto, G.; Putra, G. S.; Suhud, F. Validation of In-Vitro Bioassay Methods: Application in Herbal Drug Research. In *Profiles of Drug Substances, Excipients and Related Methodology*; Elsevier, 2021; Vol. *46*, pp 273−307.
(43) Guha, R. On Exploring Structure−Activity Relationships. In *Methods in Molecular Biology*; Kortagere, S., Ed.; Humana Press: Totowa, NJ, 2013; Vol. *993*, pp 81−94.
(44) Eramo, A.; Lotti, F.; Sette, G.; Pilozzi, E.; Biffoni, M.; Di Virgilio, A.; Conticello, C.; Ruco, L.; Peschle, C.; De Maria, R. Identification and Expansion of the Tumorigenic Lung Cancer Stem Cell Population. *Cell Death Differ.* **2008**, *15* (3), 504−514.
(45) Mohiuddin, I. S.; Wei, S.-J.; Kang, M. H. Role of OCT4 in Cancer Stem-like Cells and Chemotherapy Resistance. *Biochim. Biophys. Acta, Mol. Basis Dis.* **2020**, *1866* (4), No. 165432.
(46) Wei, Y.; Li, Y.; Chen, Y.; Liu, P.; Huang, S.; Zhang, Y.; Sun, Y.; Wu, Z.; Hu, M.; Wu, Q.; Wu, H.; Liu, F.; She, T.; Ning, Z. ALDH1: A Potential Therapeutic Target for Cancer Stem Cells in Solid Tumors. *Front. Oncol.* **2022**, *12*, No. 1026278.
(47) Holland, J. D.; Klaus, A.; Garratt, A. N.; Birchmeier, W. Wnt Signaling in Stem and Cancer Stem Cells. *Curr. Opin. Cell Biol.* **2013**, *25* (2), 254−264.
(48) Rampogu, S.; Son, M.; Baek, A.; Park, C.; Rana, R. M.; Zeb, A.; Parameswaran, S.; Lee, K. W. Targeting Natural Compounds against HER2 Kinase Domain as Potential Anticancer Drugs Applying Pharmacophore Based Molecular Modelling Approaches. *Comput. Biol. Chem.* **2018**, *74*, 327−338.
(49) Ishikawa, T.; Seto, M.; Banno, H.; Kawakita, Y.; Oorui, M.; Taniguchi, T.; Ohta, Y.; Tamura, T.; Nakayama, A.; Miki, H.;

Kamiguchi, H.; Tanaka, T.; Habuka, N.; Sogabe, S.; Yano, J.; Aertgeerts, K.; Kamiyama, K. Design and Synthesis of Novel Human Epidermal Growth Factor Receptor 2 (HER2)/Epidermal Growth Factor Receptor (EGFR) Dual Inhibitors Bearing a Pyrrolo[3,2-*d*]Pyrimidine Scaffold. *J. Med. Chem.* **2011**, *54* (23), 8030−8050.
(50) Peng, Y.-H.; Shiao, H.-Y.; Tu, C.-H.; Liu, P.-M.; Hsu, J. T.-A.; Amancha, P. K.; Wu, J.-S.; Coumar, M. S.; Chen, C.-H.; Wang, S.-Y.; Lin, W.-H.; Sun, H.-Y.; Chao, Y.-S.; Lyu, P.-C.; Hsieh, H.-P.; Wu, S.-Y. Protein Kinase Inhibitor Design by Targeting the Asp-Phe-Gly (DFG) Motif: The Role of the DFG Motif in the Design of Epidermal Growth Factor Receptor Inhibitors. *J. Med. Chem.* **2013**, *56* (10), 3889−3903.
(51) Modi, V.; Dunbrack, R. L. Defining a New Nomenclature for the Structures of Active and Inactive Kinases. *Proc. Natl. Acad. Sci. U.S.A.* **2019**, *116* (14), 6818−6827.
(52) Son, J.; Jang, J.; Beyett, T. S.; Eum, Y.; Haikala, H. M.; Verano, A.; Lin, M.; Hatcher, J. M.; Kwiatkowski, N. P.; Eser, P. Ö.; Poitras, M. J.; Wang, S.; Xu, M.; Gokhale, P. C.; Cameron, M. D.; Eck, M. J.; Gray, N. S.; Jänne, P. A. A Novel HER2-Selective Kinase Inhibitor Is Effective in HER2Mutant and Amplified Non−Small Cell Lung Cancer. *Cancer Res.* **2022**, *82* (8), 1633−1645.
(53) Almeida, T. C.; Guerra, C. C. C.; De Assis, B. L. G.; de Oliveira Aguiar Soares, R. D.; Garcia, C. C. M.; Lima, A. A.; Da Silva, G. N. Antiproliferative and Toxicogenomic Effects of Resveratrol in Bladder Cancer Cells with Different *TP53* Status. *Environ. Mol. Mutagen.* **2019**, *60* (8), 740−751.
(54) Fu, Y.; Ye, Y.; Zhu, G.; Xu, Y.; Sun, J.; Wu, H.; Feng, F.; Wen, Z.; Jiang, S.; Li, Y.; Zhang, Q. Resveratrol Induces Human Colorectal Cancer Cell Apoptosis by Activating the Mitochondrial Pathway via Increasing Reactive Oxygen Species. *Mol. Med. Rep.* **2020**, *23* (3), No. 170.
(55) Feng, M.; Zhong, L.-X.; Zhan, Z.-Y.; Huang, Z.-H.; Xiong, J.-P. Resveratrol Treatment Inhibits Proliferation of and Induces Apoptosis in Human Colon Cancer Cells. *Med. Sci. Monit.* **2016**, *22*, 1101−1108.
(56) Li, X.; Wang, D.; Zhao, Q. C.; Shi, T.; Chen, J. Resveratrol Inhibited Non−Small Cell Lung Cancer Through Inhibiting STAT-3 Signaling. *Am. J. Med. Sci.* **2016**, *352* (5), 524−530.
(57) Wright, C.; Iyer, A. K. V.; Yakisich, J. S.; Azad, N. Anti-Tumorigenic Effects of Resveratrol in Lung Cancer Cells Through Modulation of c-FLIP. *Curr. Cancer Drug Targets* **2017**, *17* (7), 669−680, DOI: 10.2174/1568009617666170315162932.
(58) Florio, R.; De Filippis, B.; Veschi, S.; Di Giacomo, V.; Lanuti, P.; Catitti, G.; Brocco, D.; Di Rienzo, A.; Cataldi, A.; Cacciatore, I.; Amoroso, R.; Cama, A.; De Lellis, L. Resveratrol Derivative Exhibits Marked Antiproliferative Actions, Affecting Stemness in Pancreatic Cancer Cells. *IJMS* **2023**, *24* (3), No. 1977.
(59) Zanoni, M.; Piccinini, F.; Arienti, C.; Zamagni, A.; Santi, S.; Polico, R.; Bevilacqua, A.; Tesei, A. 3D Tumor Spheroid Models for in Vitro Therapeutic Screening: A Systematic Approach to Enhance the Biological Relevance of Data Obtained. *Sci. Rep.* **2016**, *6* (1), No. 19103.
(60) Rozenberg, J. M.; Filkov, G. I.; Trofimenko, A. V.; Karpulevich, E. A.; Parshin, V. D.; Royuk, V. V.; Sekacheva, M. I.; Durymanov, M. O. Biomedical Applications of Non-Small Cell Lung Cancer Spheroids. *Front. Oncol.* **2021**, *11*, No. 791069.
(61) Riudavets, M.; Sullivan, I.; Abdayem, P.; Planchard, D. Targeting HER2 in Non-Small-Cell Lung Cancer (NSCLC): A Glimpse of Hope? An Updated Review on Therapeutic Strategies in NSCLC Harbouring HER2 Alterations. *ESMO Open* **2021**, *6* (5), No. 100260.
(62) Fath, M. K..; Ebrahimi, M.; Nourbakhsh, E.; Hazara, A. Z.; Mirzaei, A.; Shafieyari, S.; Salehi, A.; Hoseinzadeh, M.; Payandeh, Z.; Barati, G. PI3K/Akt/mTOR Signaling Pathway in Cancer Stem Cells. *Pathol., Res. Pract.* **2022**, *237*, No. 154010.
(63) Rivas, S.; Gómez-Oro, C.; Antón, I.; Wandosell, F. Role of Akt Isoforms Controlling Cancer Stem Cell Survival, Phenotype and Self-Renewal. *Biomedicines* **2018**, *6* (1), No. 29.
(64) Wei, Y.; Jiang, Y.; Zou, F.; Liu, Y.; Wang, S.; Xu, N.; Xu, W.; Cui, C.; Xing, Y.; Liu, Y.; Cao, B.; Liu, C.; Wu, G.; Ao, H.; Zhang, X.; Jiang, J. Activation of PI3K/Akt Pathway by CD133-P85 Interaction Promotes Tumorigenic Capacity of Glioma Stem Cells. *Proc. Natl. Acad. Sci. U.S.A.* **2013**, *110* (17), 6829−6834.

https://doi.org/10.1021/acs.chemrestox.4c00436
Chem. Res. Toxicol. 2025, 38, 415−432